Implementation and Validation of the Social Force Model for Crowd Behaviour

by

M.Q. Capelle

in partial fulfillment of the requirements for the degree of

Bachelor of Science
in Applied Physics

at Delft University of Technology,
to be defended publicly on Tuesday August 21, 2018 at 13:00.

Student number:	4268628	
Supervisor:	Assoc. prof. dr. S. Kenjeres, Dipl.-Ing	TU Delft (Transport Phenomena)
Thesis committee:	Prof. dr. ir. C. R. Kleijn	TU Delft (Transport Phenomena)

TU Delft Delft University of Technology

ABSTRACT

Crowd modelling is essential to the understanding of pedestrian logistics and prevention of crowd disasters. Agent-based approaches can realistically predict crowd behaviour. The social force model as proposed by Helbing and Mólnar in 1995[1] is a widely used agent-based approach. This is a physical model for psychological behaviour that relies strongly on its various parameter values. To investigate the underlying thought of the social force model the physical consequences of the effects and parameters are reviewed in this thesis. Next to this, an adjustment on Helbing and Mólnar's model is made by treating agents as particles with a hard kernel, requiring a walkover- and ghost-prevention functionality. In addition, it is suggested to set the agent interaction magnitude to $U^0_{\alpha\beta} = 21\ \mathrm{m}^2/\mathrm{s}^2$. Subsequently, the adjusted model is validated to empirical research done by Seyfried et al.[2] and to simulations done by Helbing and Mólnar[1]. For validation a cluster analysis method is developed to give a quantitative measure of the number of lanes.

Contents

NOMENCLATURE

A list of the symbols used in this thesis is shown in this section. For the computer simulations the values as given here are used to set the parameters, unless otherwise specified. If the value varies strongly or is irrelevant, this is denoted by '-'.

General

Symbol	Units	Value	Description
J	1/s	-	Pedestrian flow
N_α	[-]	-	Number of agents
N_L	[-]	-	Number of lanes
N_C	[-]	-	Number of clusters
Δt	s	0.1	Iteration time step size
t_{end}	[-]	3000	Last iteration step
t_{start}	[-]	0	First iteration step
W_d	m	1	Door width
x	m	0-50	X- coordinate map
X	m	17.3, 50	Corridor length
Y	m	2-20	Corridor width
y	m	0-20	Y-coordinate map
$\#t$	[-]	-	Number of iteration time steps

Agent properties

Symbol	Units	Value	Description
c_ϕ	[-]	0.5	Perception weight factor
d_α	m	0.5	Agent size
$\vec{e}_\alpha$	m	-	Moving direction of agent α
m_α	kg	-	Mass of agent α
t_α	s	0.5	Relaxation term of agent α
$\vec{r}_\alpha$	m	-	Position of agent α
$\overline{v}$	m/s	-	Average velocity over time and agents
$\langle v_0 \rangle$	m/s	1.34	Mean initial velocity
$\vec{v}_\alpha$	m/s	-	Actual velocity of agent α
v_{factor}^{max}	[-]	1.3	Maximum velocity factor
$\vec{w}_\alpha$	m/s	-	Preferred velocity of agent α
w_ϕ	[-]	-	Perception weight term
$\sqrt{\theta}$	m/s	0.26	Standard deviation of initial velocity
θ_α	deg	-	Angular position of agent α
λ	pedestrian/m^{-1}	0.4-2	Agent line density
ρ	pedestrian/m^{-2}	0.3	Agent density
ϕ	deg	100	Angle of sight

Social force effects

Symbol	Units	Value	Description
b	m	-	Semi-minor axis
$\vec{f}_\alpha^0$	m/s^2	-	Driving effect working on agent α
$\vec{f}_{\alpha\beta}$	m/s^2	-	Interaction effect induced by agent β on agent α
$\vec{f}_{\alpha B}$	m/s^2	-	Boundary effect induced by boundary B on agent α
R	m	0.2	Characteristic length of boundary effect
$U_{\alpha B}^0$	m^2/s^2	10	Boundary magnitude
$V_{\alpha\beta}^0$	m^2/s^2	21	Interaction magnitude
σ	m	0.3	Characteristic length of interaction effect

Cluster properties

Symbol	Units	Value	Description
$r_{\text{max,x}}$	m	10	Maximum x-position difference between two agents
$r_{\text{max,y}}$	m	10	Maximum y-position difference between two agents
v_{max}	m/s	1	Maximum velocity difference between two agents
e_{max}	deg	20	Maximum direction difference between two agents
W_c	m	20	Width of cluster domain
ϕ_{max}	deg	20	Maximum angle of sight for cluster analysis method

1

INTRODUCTION

Predicting crowd behaviour is essential to guarantee safety in crowded situations and in cases of emergency. Due to increased mobility and higher population densities, the number and intensity of crowded situations increases. This strengthens the urge for a reliable forecast of crowd behaviour. The need for good forecasts is painfully illustrated by the German Loveparade catastrophe in 2010. In this accident 25 people died and more than 500 were injured during an unpredicted stampede, [3].

Crowd behaviour can be predicted by different numerical models. Of these models the social force model is the most widely used and investigated, [4]. The social force model was first proposed by Helbing and Mólnar in 1995, [1]. Among others, the most recent articles on the social force model are published by Chen et al. [5] and Qu et al. [6].

The social force model is a physical model for psychological behaviour that relies strongly on its various parameter values. These parameter values are mainly retrieved by fitting empirical studies, [7]. However, just fitting parameters often misses the underlying thought that links psychological behaviour and physical motion. To investigate the underlying thought of the social force model this work attempts to answer the following question:

"What are the physical consequences of the effects and parameters of the social force model?"

This question is answered by implementing the social force model. This implementation leads to adjustments based on computational analysis and literature studies. Subsequently, the implementation is validated. For this validation a cluster analysis method is developed.

In chapter 2 the major crowd behaviour models are discussed. The social force model and the working of its social forces (effects) are discussed in more detail here. Chapter 3 elaborates on the numerical implementation of the theory and the consequences of the effects and parameters. Improvements to Helbing and Mólnar's model are made in this chapter. In addition, the developed cluster analysis method is explained here. Chapter 4 shows the quantitative and qualitative validation of the implemented model by comparing it to results found by Helbing and Mólnar [1] and Seyfried et al. [2]. In chapter 5 all conclusions and assumptions made in this thesis are given. This chapter also includes suggestions for further research.

2

THEORY

In this chapter the main theory regarding crowd modelling is discussed. In section 2.1 a description of pedestrian behaviour characteristics is given. After this, the seven major crowd modelling approaches are shortly discussed in section 2.2. Finally, the social force model is discussed in more detail in section 2.3.

2.1. CROWD MODELLING

2.1.1. COLLECTIVE EFFECTS

A large variety of self-organising phenomena and collective effects are observed in empirical pedestrian dynamic studies. These effects stem from individual decisions influenced by microscopic interactions and individual desires, [8], [9]. Schadschneider et al. describe a decision making process that leads to pedestrian motion, [10]. This decision process consists of three levels of behaviour. First, at the strategic level main choices of activities are made. Second, the tactical level describes short-term decisions based on other pedestrians, obstacles, etc. Third, the operational level defines the actual walking behaviour by making immediate decisions, e.g. to avoid collisions, [10].

Schadschneider et al.[10] distinguishe six collective effects: (1) jamming, (2) density waves, (3) lane formation, (4) oscillations, (5) patterns at intersections, and (6) emergency situations and 'panic'. The first effect, jamming, occurs at high densities at locations with reduced capacity, so called 'bottle necks.' Examples are narrowings and exits. The second effect, density waves, are quasi-periodic density variations in space and time. Moreover, at high densities a crowd can behave like a fluid mass, [11]. Third, Schadschneider mentions lane formation. Lane formation happens when groups move in opposite directions, so called counterflow. Moving in lanes reduces strong interactions with oncoming pedestrians, [12]. Interestingly, this effect shows resemblances with mindless particles, [13].

Another collective effect mentioned by Schadschneider et al. are oscillations. In counterflow at locations with reduced capacity pedestrians can show oscillatory changes in moving direction. Fifth, various collective motion patterns can be observed at intersections. These patterns can allow for a smoother motion. Finally, Schadschneider discusses emergency situations and 'panic'. Although panic is sometimes assumed to result in selfish, asocial, or even irrational behaviour, this kind of panic is not often observed, [10], [14].

2.1.2. FLOW, DENSITY AND THE FUNDAMENTAL DIAGRAM

In the field of crowd behaviour modelling the most commonly used observables are pedestrian flow J and pedestrian density ρ, [10]. The flow J is defined as the number of pedestrians crossing a fixed location per unit of time, see equation 2.1. On way to find J is by determining the times t_i at which pedestrians pass the location. The flow is directly related to the time gaps $\Delta t_i = t_{t+1} - t_i$ between two pedestrians i and $i+1$.

$$J = \frac{1}{\langle \Delta t_i \rangle} \tag{2.1}$$

with $\langle \Delta t_i \rangle$ the average time gap for N pedestrians:

$$\langle \Delta t_i \rangle = \frac{1}{N} \sum_{i=1}^{N} (t_{i+1} - t_i) = \frac{t_{N+1} - t_i}{N}. \tag{2.2}$$

Fluid dynamics offer another way to measure the pedestrian flow. In this case flow is given by

$$J = \rho \overline{v} b = J_s b. \tag{2.3}$$

Where ρ [pedestrian/m] is the average pedestrian density, $\overline{v}$ [m/s] the average speed and b [m] the width of the facility. J_s is the specific flow and gives the flow per unit-width.

When agents walk in one line, the flow can be calculated from the agent line density λ [pedestrian/m] and the average velocity $\overline{v}$ of all agents according to

$$J = \lambda \overline{v}. \tag{2.4}$$

The pedestrian density ρ can be calculated via multiple ways, [10]. Fruin proposed to quantify pedestrian load using the reciprocal of the density: the 'pedestrian area module', [11]. Continuing on Fruin, the inter-person distance d was introduced by Thompson and Marchant. They defined the average inter-person distance as $\langle d \rangle = \sqrt{1/\rho}$, [15].

2.2. CROWD MODELLING APPROACHES

Numerous crowd behaviour modelling approaches exist. These techniques differ in their ability to correctly simulate collective effects. Zheng et al.[4] list seven approaches of crowd modelling using 1) a cellular automata model, 2) a lattice gas model, 3) a social force model, 4) fluid-dynamics, 5) an agent-based model, 6) game theoretics, and 7) animals. These approaches are shortly discussed later in this section.

In general, crowd behaviour models can be categorised using different features. The main feature are the three classical types of scale: microscopic, mesoscopic and macroscopic, [16]. In models on microscopic scale, each pedestrian is represented separately and with individual characteristics, like preferred velocity or behaviour. Interactions between pedestrians can be shown on this scale. In a mesoscopic scale model a probability distribution over the microscopic state of pedestrians is used to find the corresponding dynamics. In macroscopic scale models individuals cannot be distinguished. These models show general quantities, like densities and average momentum, [16].

In addition, modelling approaches can also be categorised by distinguishing in space and time i.e. discrete or continuous, and whether individuals or groups are shown, i.e. homogeneous or heterogeneous, [4]. Distinguishing whether a model is applicable for normal or emergency situations is not relevant, because most models are applicable for both situations, [4]. An overview of all properties can be found in table 2.1.

Approach	Scale	Space and time	Individuals/groups
Cellular automata	Microscopic	Discrete	Both
Lattice gas	Microscopic	Discrete	Homogeneous
Social force	Microscopic	Both	Homogeneous
Fluid-dynamics	Macroscopic	Continuous	Homogeneous
Agent-based	Microscopic	Both	Heterogeneous
Game theoretic	Microscopic	Discrete	Homogeneous
Animals	Microscopic	-	Homogeneous

Table 2.1: Overview of the characteristics of crowd modelling approaches.

CELLULAR AUTOMATA MODELS

Cellular automata models are microscopic and discrete, and can be either homogeneous or heterogeneous. These type of models use a discrete dynamic system in which space is divided in a uniform grid.

Zheng discusses two categories of cellular automata models, [4]. The first category is based on interactions between pedestrians and their environments. The second is based on interactions between pedestrians only. The last type can be used to study friction between pedestrians [17], bidirectional behaviour [18] and herding behaviour [19]. Cellular automata can be combined with other approaches, such as the social force model [20] or the lattice gas approach [21].

LATTICE GAS MODELS

A special case of cellular automata are lattice gas models. These models are homogeneous, microscopic and discrete. The crowd behaviour is modelled using probability and statistics. This type of model can give insight in the flow of pedestrians, [4].

SOCIAL FORCE MODEL

The social force model is homogeneous, microscopic and either continuous or discrete. In the social force model, individual agents make decisions based on four effects ('forces'): 1) a desire to reach a certain destination and stick to a certain desired velocity, the desire to keep a certain distance from 2) other agents and 3) boundaries, and 4) attraction by other agents or objects, [1]. This model is discussed in more detail in section 2.3.

FLUID-DYNAMICS

The fluid-dynamic model is homogeneous, macroscopic and continuous. This model can be used at medium to high pedestrian densities. For example, Helbing mentions that the stream of pedestrians through a crowd shows resemblances with riverbeds, [22].

Hughes developed a model based on partial differential equations to describe how velocity and density change over time. This model is based on the following three hypothesises:

1. "The speed at which pedestrians walk is determined solely by the density of surrounding pedestrians, the behavioural characteristics of the pedestrians, and the ground on which they walk.

2. Pedestrians have a common sense of the task (called potential) that they face to reach their common destination, such that any two individuals at different locations having the same potential would see no advantage to exchanging places.

3. Pedestrians seek to minimize their (accurately) estimated travel time but temper this behavior to avoid extreme densities. This tempering is assumed to be separable, such that pedestrians minimize the product of their travel time as a function of density." [23, p. 171]

From these hypothesises he derived the governing equations for pedestrian motion as stated in equations 2.5 and 2.6.

$$-\frac{\partial \rho}{\partial t}+\frac{\partial}{\partial x}\left(\rho g(\rho) v^2(\rho)\frac{\partial \phi}{\partial x}\right)+\frac{\partial}{\partial y}\left(\rho g(\rho) v^2(\rho)\frac{\partial \phi}{\partial y}\right)=0 \tag{2.5}$$

$$g(\rho) v(\rho)=\frac{1}{\sqrt{\left(\frac{\partial \phi}{\partial x}\right)^2+\left(\frac{\partial \phi}{\partial y}\right)^2}}. \tag{2.6}$$

With ϕ the remaining travel time, called 'potential' as ϕ is a measure for the remaining task. ρ is the density of the crowd, $v(\rho)$ the speed of pedestrians and $g(\rho)$ a factor of discomfort. (x, y, t) denote the horizontal space and time coordinates.

AGENT-BASED MODELLING

Agent-based models are heterogeneous, microscopic and can be either continuous or discrete. The possibility to give each agent unique characteristics enables a more realistic heterogeneous crowd simulation. However, agent-based models require more computational efforts than continuous models. Some agent-based models are based on the social force model[24] or the cellular automata model[25]. Agent-based models appear to be valuable for especially panic and jamming simulations, [26].

GAME THEORETIC

The game theoretic approach assumes pedestrians behave according to a rational decision making process. In a game, pedestrians can access all available options and then select their most favourable option. This model can test pedestrian interaction, [4].

ANIMALS

Finally, animals can be used to simulate crowd behaviour in panic situations. These simulation techniques show that panic can propagate by imitation, [4].

2.3. SOCIAL FORCE MODEL

In this section the social force model will be discussed in more detail, based on the article by Helbing and Mólnar, [1]. First, the social force model is introduced shortly. Subsequently, the four main effects will be discussed. After this, the consequences of the so called effective angle of sight are discussed. Finally, the relation between the effects and the motion of an agent is explained.

A short note on definitions is in it's place here. In this thesis, 'real world' human pedestrians are indicated with the term 'pedestrians' whereas the term 'agent' refers to computer simulated individuals. Next to this, in literature the effects are denoted both with upper case F and lower case f. In this thesis, F is used for forces only and f for effects.

2.3.1. INTRODUCTION

The social force model for pedestrian motion was proposed by Helbing and Mólnar in 1995, [1]. The social force model is still widely used today, [27]. According to this model, pedestrian movement is fully determined by four effects. First, the driving effect $\vec{f}_\alpha^0$ represents agent α's desire to reach a certain destination and stick to a certain desired velocity v_α^0. Second, an agent wants to keep a certain distance from other agents, resulting in the interaction effect $\vec{f}_{\alpha\beta}$. Next to this, the preference to keep a certain distance from boundaries results in a third force: the boundary effect $\vec{f}_{\alpha B}$. Finally, attraction by other persons (e.g. friends) and objects (e.g. windows) results in the interaction effect $\vec{f}_{\alpha i}$, [1].

For this thesis, the social force model is used because of its versatile and adaptable features. As first advantage, the social force model explicitly calls upon distinguishable effects ('forces'). As a consequence, the influence and physical interpretation of these effects can easily be investigated separately. Second, the agent-based approach enables customisation of agents' individual characteristics. Thanks to this property, a computer model can be extended easily to give more realistic predictions. Third, the social force model can be combined with other models. For example, Guo and Huang created a lattice gas model based on the social force model, [28]. The cellular automata [20] and multi-grid model [29] are based on the social force model too. Fourth, the social force model is prominent among a broad range of researchers, [4]. This popularity partly stems from its agent-based approach and its connection with other models, making the social force model widely applicable.

Despite its name, the social force model actually works with effects instead of forces. However, these effects are treated similar to forces in Newton's second law for the equation of movement. The effects in the social force model influence the agent's decisions, resulting in a certain motion. Hereby it is assumed that equation 2.7 holds and that the agent's mass m_α stays constant during the simulation. Subsequently, the effect f can be seen as an acceleration term.

$$\vec{F} = m_\alpha \vec{f} \tag{2.7}$$

2.3.2. DRIVING EFFECT

The driving effect $\vec{f}_\alpha^0$ ensures that agent α has a motion that is in accordance with the agent's desired velocity v_α^0 and has a direction $\vec{e}_\alpha^0$ towards its desired destination:

$$\vec{f}_\alpha^0(\vec{v}_\alpha, v_\alpha^0 \vec{e}_\alpha) = \frac{v_\alpha^0 \vec{e}_\alpha^0 - \vec{v}_\alpha}{t_\alpha} \tag{2.8}$$

The driving effect scales linearly with $1/t_\alpha$. A lower relaxation term makes the agent more aggressive, having a larger $\vec{f}_\alpha^0$. If no other effects apply, the agent will need t_α seconds to reach its ideal velocity $\vec{v}_\alpha^0$. When the magnitude of the agent's actual velocity $\vec{v}_\alpha$ is larger than its desired velocity v_α^0, the driving effect will slow the agent down. When the agents actual velocity is smaller than its desired velocity, the reverse applies.

Next to the magnitude correction, the driving effect takes the desired direction into account. When an agent moves in a direction that is not straight to its destination, the driving effect tends to pull the agent's motion towards its destination. In figure 2.1 the driving effect is shown for an agent with an actual velocity that does not point towards its desired destination but to the right. The direction changing effect can be explained by treating the driving effect similar to a force, and writing down the vector of the force explicitly in its x and y components:

$$\begin{bmatrix} F_x^0 \\ F_y^0 \end{bmatrix} = \frac{\mathrm{d}}{\mathrm{d}t} m_\alpha \begin{bmatrix} v_\alpha^0 e_{\alpha x}^0 - v_{\alpha x} \\ v_\alpha^0 e_{\alpha y}^0 - v_{\alpha y} \end{bmatrix}.$$

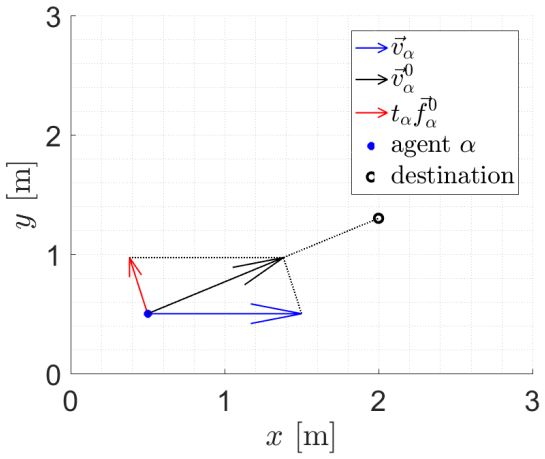

Figure 2.1: Driving effect (red) for agent α (blue dot) with an actual velocity $\vec{v}_\alpha$ (blue arrow) that is not towards the desired destination (black circle). The driving effect 'pulls' the agent's motion towards its destination. The driving effect is multiplied with the relaxation time t_α to retrieve equal dimensions (m/s).

2.3.3. BOUNDARY EFFECT

Pedestrians tend to keep a certain distance from boundaries like walls, streets and obstacles. Closer to a boundary, the agent has to pay more attention not to get hurt and consequently feels more uncomfortable. This results in a repulsive effect described by the boundary effect as defined in equation 2.9. The generated repulsive effect points away from the boundary, as follows from the divergence $-\nabla_{\vec{r}_{\alpha B}}$.

$$\vec{f}_{\alpha B}(\vec{r}_{\alpha B}) = -\nabla_{\vec{r}_{\alpha B}} U_{\alpha B}(||\vec{r}_{\alpha B}||). \tag{2.9}$$

Here, $U_{\alpha B}(||\vec{r}_{\alpha B}||)$ is the repulsive potential that decreases exponentially with the distance between agent α and the part of boundary B closest to agent α, $||\vec{r}_{\alpha B}||$, see equation 2.10. The exponential decay is illustrated in figure 2.2 for characteristic length $R = 0.2$ m and boundary magnitude $U^0_{\alpha B} = 10\text{m}^2/\text{s}^2$.

$$U_{\alpha B}(||\vec{r}_{\alpha B}||) = U^0_{\alpha B} e^{-||\vec{r}_{\alpha B}||/R} \tag{2.10}$$

Repulsive effects directed parallel to the boundary, $f_{\alpha B,\parallel}$, are not taken into account. To clarify this, it is assumed that the walls have an infinite length in the y-direction by virtue of periodic boundary conditions. In this case, every repulsive effect generated by boundary δB at a distance δ from one side of agent α is cancelled by a repulsive effect generated by boundary $\delta B'$ at an equal distance δ from the other side of agent α. As the repulsive effect is approximately zero at $||\vec{r}_{\alpha B}|| \geq 1$ m, this assumption can be applied to boundaries with finite length, provided that the agent is not too close to one edge of the wall.

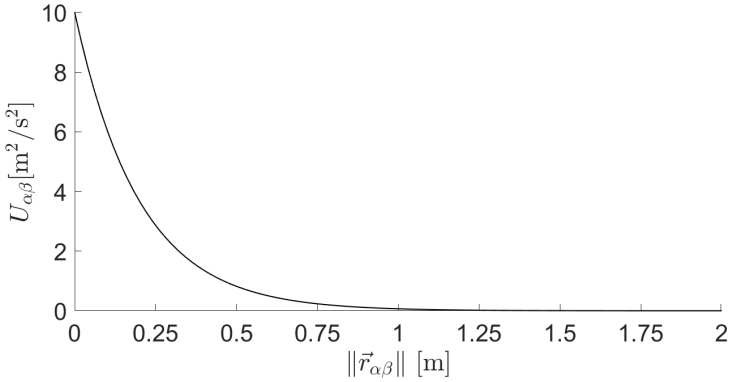

Figure 2.2: The repulsive potential $U_{\alpha B}$ generated by boundary B on agent α, for $R = 0.2$ m and $U^0_{\alpha B} = 10\text{m}^2/\text{s}^2$. $U_{\alpha B}$ decays exponentially with $\|\vec{r}_{\alpha B}\|$. Note $\vec{f}_{\alpha B}(\|\vec{r}_{\alpha B}\| \geq 1\text{m}) \approx 0$.

2.3.4. INTERACTION EFFECT

In general, a pedestrian feels increasingly uncomfortable when another (unknown) pedestrian comes closer into his private sphere. Due to this effect pedestrians tend to keep a certain distance from other pedestrians. This repulsive effect is given by the vectorial quantities in equation 2.11.

$$\vec{f}_{\alpha\beta}(\vec{r}_{\alpha\beta}) = -\nabla_{\vec{r}_{\alpha\beta}} V_{\alpha\beta}\left[b\left(\vec{r}_{\alpha\beta}\right)\right] \tag{2.11}$$

The closer a pedestrian comes to a stranger, the stronger the repulsive effect $\vec{f}_{\alpha\beta}$ will be. This effect scales with repulsive potential $V_{\alpha\beta}$, similar to the boundary potential $U^0_{\alpha\beta}$. Helbing defines a decreasing repulsive potential as:

$$V_{\alpha\beta}\left[b\left(\vec{r}_{\alpha\beta}\right)\right] = V^0_{\alpha\beta} e^{-b/\sigma}. \tag{2.12}$$

In this potential σ is the characteristic length for the interaction potential, defined as $\sigma = 0.3$ m. b denotes the semi-minor axis of an ellipse, taking into account both the distance between agent α and agent β, ($\|\vec{r}_{\alpha\beta}\|$), and the velocity of agent β, $\vec{v}_\beta$. When agent β has a higher velocity, he will need more space for the next step $s_\beta = v_\beta \Delta t$, increasing b. The distance between the agents is defined as $\vec{r}_{\alpha\beta} = \vec{r}_\alpha - \vec{r}_\beta$. In equation 2.13 the definition of b is given.

$$2b = \sqrt{\left(\left|\left|\vec{r}_{\alpha\beta}\right|\right| + \left|\left|\vec{r}_{\alpha\beta} - \vec{v}_\beta \Delta t\right|\right|\right)^2 - \left(\vec{v}_\beta \Delta t\right)^2}. \tag{2.13}$$

The interaction effect is illustrated in figure 2.3. Initially, the agents are distributed closely to each other at $\#t = 1$. Due to the interaction effect, the agents move away from each other. As the mutual distances increase, the interaction effect becomes lower and the agents start to move more slowly ($\#t = 1$ to $\#t = 10$). In this figure, the agents cannot move through the boundary but do not feel any boundary repulsion.

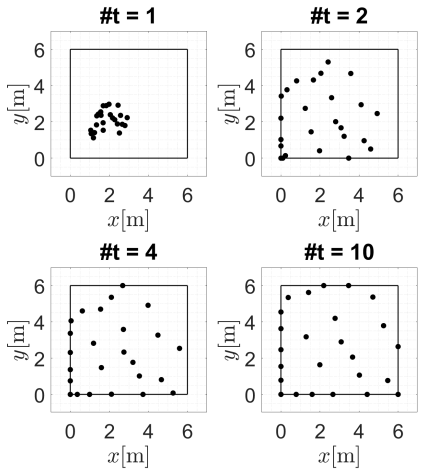

Figure 2.3: Due to the interaction effect agents move away from each other. The agents cannot move through the boundary but do not feel any boundary repulsion.

2.3.5. ATTRACTIVE EFFECT

Next to repulsion, pedestrians can also be attracted to objects (e.g. windows) or other pedestrians (e.g. friends). Helbing defines attractive effects as in equation 2.14.

$$\vec{f}_{\alpha i}\left(\left|\left|\vec{r}_{\alpha i}\right|\right|, t\right) = -\nabla_{\vec{r}_{\alpha i}} W_{\alpha i}\left(\left|\left|\vec{r}_{\alpha i}\right|\right|, t\right) \tag{2.14}$$

With $\vec{r}_{\alpha i} = \vec{r}_\alpha - \vec{r}_i$ the distance between agent α and object i. The magnitude of the attractive effect $\|\vec{f}_{\alpha i}\|$ declines with time t as an agent loses its interest in object i. As the attractive effect is neglected in most elementary models, it is not taken into account for the simulations of this thesis.

2.3.6. EFFECTIVE ANGLE

Both the interaction effect and attractive effect are stronger for objects that are perceived in the moving direction $\vec{e}_\alpha$ than objects that are behind agent α. To take this difference into account, Helbing introduces the perception weight term w_ϕ. Here, 2ϕ is the effective angle of sight and c_ϕ is the weight factor for situations outside the effective angle of sight, with $0 < c_\phi < 1$. Consequently, w_ϕ is defined as in equation 2.15.

$$w_\phi(\vec{e}, \vec{f}) = \begin{cases} 1 & \text{if } \vec{e} \cdot \vec{f} \leq \|\vec{f}\| cos(\phi) \\ c_\phi & \text{otherwise} \end{cases} \tag{2.15}$$

For the interaction effect $\vec{f}_{\alpha\beta}$ and respectively the attraction effect $\vec{f}_{\alpha i}$ this results in

$$\vec{f}_{\alpha\beta}(\vec{e}_\alpha, \vec{r}_\alpha - \vec{r}_\beta) = w_\phi(\vec{e}_\alpha, -\vec{f}_{\alpha\beta})\vec{f}_{\alpha\beta}(\vec{r}_\alpha - \vec{r}_\beta) \tag{2.16}$$

and

$$\vec{f}_{\alpha i}(\vec{e}_\alpha, \vec{r}_\alpha - \vec{r}_i, t) = w_\phi(\vec{e}_\alpha, \vec{f}_{\alpha i})\vec{f}_{\alpha i}(\vec{r}_\alpha - \vec{r}_i, t). \tag{2.17}$$

2.3.7. EFFECTS TO MOTION

The sum of the four effects results in the movement of an agent according to Newton's second law:

$$\sum \vec{F} = \frac{\mathrm{d}\vec{p}}{\mathrm{d}t} = \frac{\mathrm{d}m\vec{v}}{\mathrm{d}t}.$$

Helbing and Mólnar assume that all effects influence the agent's decision making on the same time, [1]. Therefore, the total effect can be obtained by summing all effects. In addition, two more assumptions are made. First, the mass m_α of each individual agent can be regarded constant. Second, the sum of the four effects $\vec{f}$ is related to force by $\vec{F} = m\vec{f}$. This results into an adjustment of Newton's second law to:

$$\sum \vec{f}_\alpha = \frac{\mathrm{d}\vec{v}_\alpha}{\mathrm{d}t}. \tag{2.18}$$

Subsequently an equation of motion for agent α can be set up by summing all effects:

$$\vec{f}_\alpha(t) = \vec{f}_\alpha^0 + \sum_\beta \vec{f}_{\alpha\beta} + \sum_B \vec{f}_{\alpha B} + \sum_i \vec{f}_{\alpha i}. \tag{2.19}$$

Agent α's preferred velocity w_α follows from the sum of all effects and an optional fluctuation term, see equation 2.20. This fluctuation term represents random behaviour variations. Random fluctuations play a role when two decisions are equivalent, e.g. deciding whether to pass an obstacle to the left or right-hand side. In Helbing and Mólnar's simulations fluctuations are considered to be 0, [1].

$$\frac{\mathrm{d}\vec{w}_\alpha}{\mathrm{d}t} = \vec{f}_\alpha(t) + \text{fluctuations} \tag{2.20}$$

Subsequently, the new preferred velocity $\vec{w}_\alpha(t + \Delta t)$ is determined by calculating the change of the actual velocity $\vec{v}_\alpha(t)$ due to the total effect $\vec{f}_\alpha(t)$:

$$\vec{w}_\alpha(t + \Delta t) = \vec{f}_\alpha(t)\Delta t + \vec{v}_\alpha(t). \tag{2.21}$$

Every agent is limited to a maximum acceptable speed v_α^{max}. This velocity maximum is implemented using a cut off for the actual velocity $\vec{v}_\alpha$ from the preferred velocity $\vec{w}_\alpha$, according to equation 2.22. Here the unit vector $\hat{w}_\alpha$ is defined as $\hat{w}_\alpha = \vec{w}_\alpha / \|\vec{w}_\alpha\|$.

$$\vec{v}_\alpha(t + \Delta t) = \begin{cases} v_\alpha^{max}\hat{w}_\alpha(t + \Delta t) & \|\vec{w}_\alpha(t + \Delta t)\| \leq v_\alpha^{max} \\ \vec{w}_\alpha(t + \Delta t) & \text{otherwise} \end{cases} \tag{2.22}$$

The position of agent α is described by the vector $\vec{r}_\alpha$. Helbing and Mólnar define this position $\vec{r}_\alpha$ by

$$\frac{\mathrm{d}\vec{r}_\alpha}{\mathrm{d}t} = \vec{v}_\alpha(t). \tag{2.23}$$

This results in the new position of every agent α. This position is calculated for every iteration time step as follows:

$$\vec{r}_\alpha(t + \Delta t) = \vec{v}_\alpha(t)\Delta t + \vec{r}_\alpha(t). \tag{2.24}$$

3

NUMERICAL IMPLEMENTATION

In this chapter the implementation of the social force model is discussed. For this, the influences of main parameters are analysed and some suggestions for adjustments are made. The current challenge in the field of crowd dynamics is parameter calibration, [7]. Therefore, the aim of this chapter is not to give any hard quantitative suggestions, but to understand the influences of parameters in a qualitative way.

The developed simulation script roughly consists of four parts: 1) dashboard, 2) initiation, 3) calculations, and 4) processing. In the so-called dashboard the properties of the simulation can be assigned, e.g. simulating uni- or bidirectional flow. The initiation part is discussed in section 3.1, containing map and boundary creation, and initial agent characteristics. In addition, the iteration step size and convergence of the model are discussed here. The actual calculations are discussed in section 3.2. Among others, the influence of parameters is investigated and adjustments on Helbing and Mólnar's [1] model are given. Section 3.3 discusses the processing part of the simulation script, including a developed model for cluster analysis and the calculation of average velocity and flow. Unless otherwise specified, parameters have values as indicated in the Nomenclature.

3.1. INITIATION

3.1.1. MAP

All simulations in this thesis are situated in a two-dimensional corridor. The dimensions of this corridor can be varied freely, provided that the corridor keeps a rectangular shape. A schematic overview of this corridor is given in figure 3.1. The corridor has a width Y and is build up by two walls with length X. One wall spans from (x_{min}, y_{min}) to (x_{max}, y_{min}) and another from (x_{min}, y_{max}) to (x_{max}, y_{max}). Two walls with a door-like opening can be added. These walls are halfway the corridor, at $(x_{max} - x_{min})/2$. The opening between these walls is exactly at the centre of the corridor, and has a width w_d. All walls are considered to have a sectional width of 0 m. To simulate the results found by Helbing and Mólnar [1], the length of the corridor is set to $X = 50$ m. The width Y is varied between 2 and 20 m. For the simulation of the experiment done by Seyfried et al.[2], the corridor is considered to be a path with length $X = 17.3$ m, without any walls.

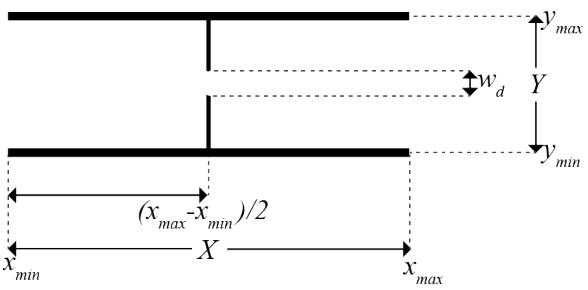

Figure 3.1: 2D corridor with walls spanning from (x_{min}, y_{min}) to (x_{max}, y_{min}), and (x_{min}, y_{max}) to (x_{max}, y_{max}). Two walls with a door-like opening of width w_d can be added.

3.1.2. ITERATION TIME STEP SIZE

High values of Δt need to be avoided, as this causes extreme displacement of agent α. In figure 3.2 the effects of Δt on the driving effect are illustrated. In all cases, agent α initially moves with its desired speed v_α^0 towards the positive x-direction and has relaxation time $t_\alpha = 0.5$ s. For $\Delta t = 1$ s the agent's steps are to large, resulting in an oscillation around the destination. At $\Delta t = 0.5$ s the agent does approach its goal in the correct direction but experiences an overshoot, overrunning its goal. For $\Delta t = 0.1$ s and $\Delta t = 0.01$ s the agent moves towards its goal. The ideal value of Δt depends on other parameters, including relaxation time t_α, boundary potential amplitude $U_{\alpha B}^0$ and interaction potential amplitude $V_{\alpha\beta}^0$.

Helbing and Mólnar use a iteration time step size $\Delta t = 2$ s, [1]. The choice for this value is not clarified. However, more modern studies use smaller time steps, e.g. [5] and [6]. Based on these studies and the computational analysis shown in figure 3.2, this thesis uses iteration time step of $\Delta t = 0.1$ s.

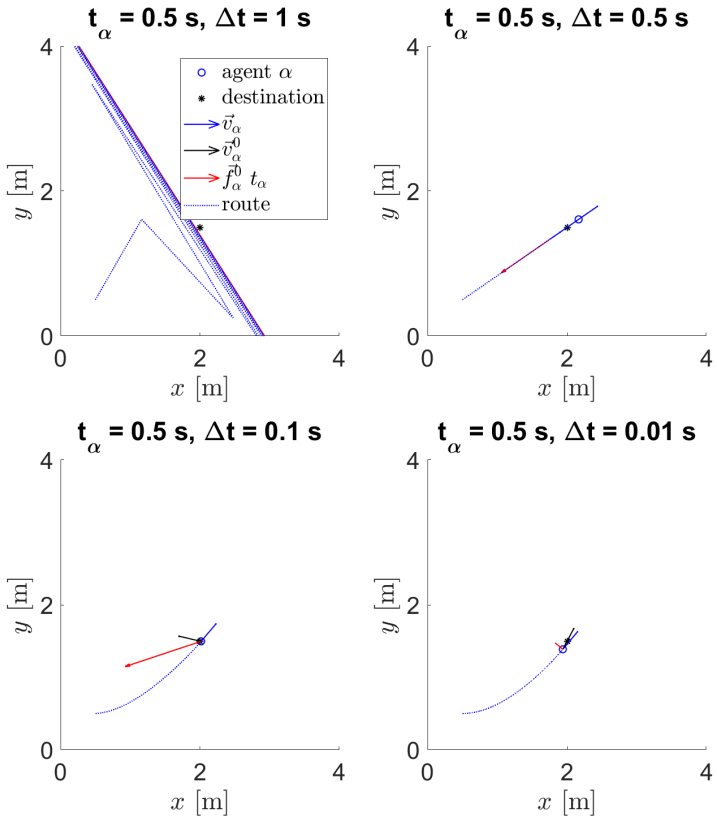

Figure 3.2: Agent motion for different iteration step sizes Δt. When Δt is too high, the agent shows overshooting behaviour (upper images.) In all cases, agent α initially moves with desired speed v_α^0 in the positive x-direction, and has the same relaxation time $t_\alpha = 0.5$ s.

3.1.3. CONVERGENCE

The simulation model converges after approximately $\#t = 1000$ iterations. From this point the absolute sum of all effects for every agent stays around the same level, as can be seen in figure 3.3. This implies that agents do not feel any sudden strong attractions or repulsions from their environment and subsequently are in a stable motion. Therefore, the agents' position relative to other agents stays roughly the same. Taking this into account, all simulations are run for minimal $\#t = 1000$ iterations, namely $\#t = 1500$. To calculate any averages over time a time domain starting at $\#t = 1500$ iterations is taken.

3.1.4. AGENT PROPERTIES

In the initiation phase the number of agents is calculated based on the agent density. Subsequently, the initial distribution, goal, and desired velocity of every agent is determined.

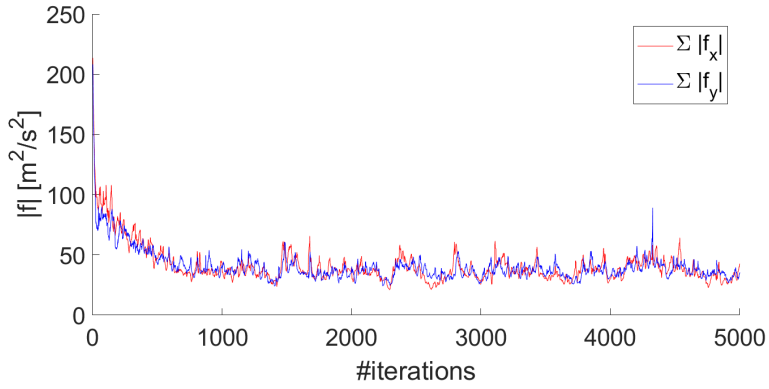

Figure 3.3: Absolute sum of all effects for different iterations. After approximately 1000 iterations the values of $\|f_x\| = \Sigma_i \|f_{x,i}\|$ and $\|f_y\| = \Sigma_i \|f_{y,i}\|$ roughly stay around the same level for both the x (red line) and y (blue line) direction. From this point, the agents' motion is stable and therefore the model has converged.

NUMBER OF AGENTS

The number of agents N_α is determined by equation 3.1. With ρ the agent density, and X and Y respectively the length and the width of the corridor in [m]. Unless otherwise specified, the agent density is set to $\rho = 0.3$ pedestrian m^{-2} as used by Helbing and Mólnar, [1].

$$N_\alpha = \rho X Y \tag{3.1}$$

The experiment done by Seyfried et al.[2] is mimicked by altering the number of agents to get line densities varying between $\lambda = 0.5$ pedestrian m^{-1} and $\lambda = 2$ pedestrian m^{-1}. The agent line density λ is calculated according to equation 3.2.

$$\lambda = \frac{N_\alpha}{X} \tag{3.2}$$

The computational time of the model is strongly influenced by the number of agents, mainly because the number of agent interactions is proportional to $N_\alpha(N_\alpha - 1)$.

AGENT DISTRIBUTION

Initially all agents are randomly distributed inside the corridor, using MATLAB's rand-function. This is shown in figure 3.4. To simulate Helbing and Mólnar's[1] door-environment another starting configuration is used. Here, all agents moving to the right respectively left start on a random position on the left respectively right half side of the corridor, see figure 3.5.

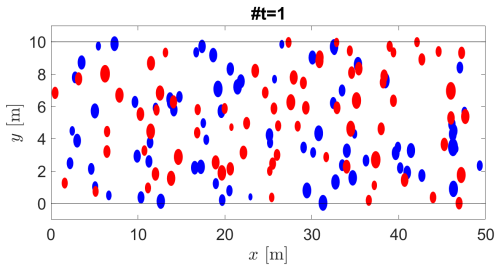

Figure 3.4: Initially all agents are randomly distributed inside the corridor. The blue respectively red agents move to the right respectively to the left. The size of every circle represents the agent's velocity.

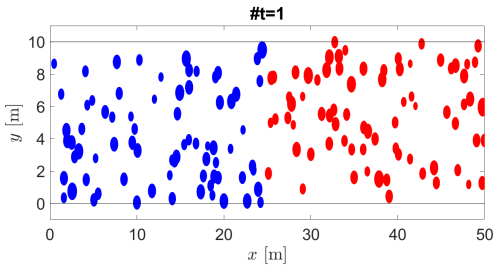

Figure 3.5: To simulate Helbing and Mólnar's[1] door-environment all agents moving to the right (blue) start on the left half side of the corridor, the agents moving towards the left (red) start on the right half side. The size of every circle represents the agent's velocity.

AGENT GOAL

For every agent an individual goal is assigned. The driving effect pulls the agent towards this goal, as described in section 2.3.2. For bidirectional flow, agents $1, 2 \ldots N_\alpha/2$ have a goal with x-coordinate x_{max}. The other half

of the agents, $N_\alpha/2, N_\alpha/2+1 \ldots N_\alpha$ have a goal with x-coordinate x_{min}. For unidirectional flow all agents $1,2,\ldots N_\alpha$ have a goal with x-coordinate x_{max}. For both uni- and bidirectional flow the y-coordinate of the goal is equal to the current y-coordinate of the agent. As the goal's function is simply to pull the agent to the other side, the y-coordinate of the agent's goal is set equal to the agent's current y-position at every iteration.

AGENT VELOCITY

In Helbing and Mólnar's social force model every agent α has its own desired speed v^0_α. The desired speeds are Gaussian distributed with mean $\langle v^0 \rangle = 1.34$ m/s and standard deviation $\sqrt{\theta} = 0.26$ m/s. The maximum acceptable velocity is set at $1.3\,v^0_\alpha$, [1]. In the simulation model all agents start with their desired speed towards their desired direction.

At high standard deviations group forming is observed. Agents with a high desired velocity are slowed down by agents in front of them, as can be seen in figure 3.6 where $\sqrt{\theta} = 1$ m/s. For comparison all agents have equal speed for $\sqrt{\theta} = 0$ m/s and subsequently form smooth lanes in figure 3.7. In both figures, all parameters are equal except for the standard deviation $\sqrt{\theta}$.

This behaviour is in line with the 'faster-is-slower' observation. Usually, the collective velocity is faster when pedestrians adjust their velocity to their fellow pedestrians, [30].

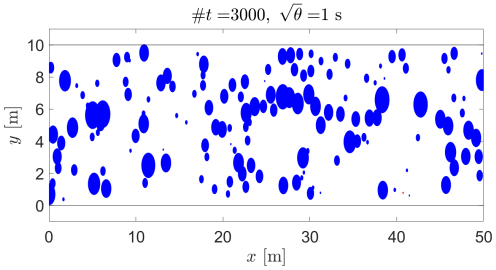

Figure 3.6: Group forming at high velocity standard deviation $\sqrt{\theta} = 1$ m/s. Agents move to the right. Faster agents get stuck behind slower predecessors. The size of a circle represents the agent's velocity.

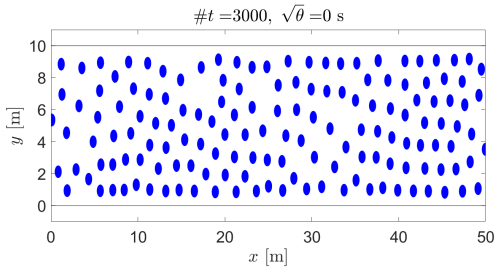

Figure 3.7: All agents have equal velocity for $\sqrt{\theta} = 0$ m/s, resulting in lane formation. The size of a circle represents the agent's velocity.

3.2. CALCULATIONS

3.2.1. DRIVING EFFECT

An important parameter in the driving effect is the relaxation term t_α as the driving effect scales linearly with $1/t_\alpha$, as discussed in section 2.3.2. Consequently, a lower relaxation term makes the agent more aggressive as the agent is more inclined to maintain its desired direction and velocity. The effect of different values of t_α is shown in figure 3.8. Starting upper left with $t_\alpha = 0.05$ s, the agent starts oscillating around its desired direction. At $t_\alpha = 0.5$ s, the agent moves more smoothly towards its goal without overshooting. For too high values of t_α the driving effect is too weak and the agent spirals around its goal. $t_\alpha = 0.5$ s is conform Helbing and Mólnar[1] and many other studies (e.g. [5],[6]). In thesis thesis the relaxation time is set to $t_\alpha = 0.5$ s. More information about the relaxation parameter the author refers to [31].

3.2.2. BOUNDARY AND INTERACTION EFFECT

The generic form of both the interaction effect and boundary effect is given in equation 3.3.

$$\vec{f} = -\nabla_{\vec{r}_{\alpha j}} A\, e^{-R_{\alpha j}/c} \tag{3.3}$$

The term $-\nabla_{\vec{r}_{\alpha j}}$ $\left[\mathrm{m}^{-1}\right]$ ensures that the effect working on agent α is directed away from object j, with $\vec{r}_{\alpha j}$ defined as $\vec{r}_\alpha - \vec{r}_j$. A $\left[\mathrm{m}^2/\mathrm{s}^2\right]$ is an amplification term: a higher value automatically results in a stronger effect, as $\|\vec{f}\| \propto A$. In the boundary effect this term is denoted by the boundary magnitude $U^0_{\alpha B}$ and in the interaction effect this term is denoted by the interaction magnitude $V^0_{\alpha\beta}$. $R_{\alpha j}$ [m] is a measure for the position difference between agent α and object j. Consequently, the effect becomes stronger when agent α moves closer to object j. The characteristic length c [m] is a measure for the rate of the exponential decay. Higher values of c result in a faster decay.

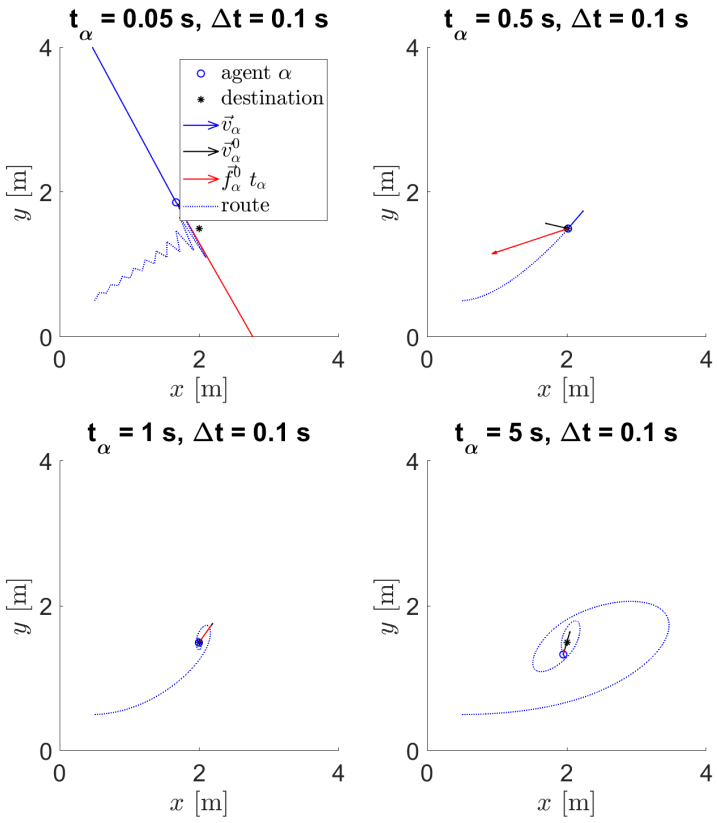

Figure 3.8: Agent motion for different values of relaxation term t_α. In all cases, agent α initially moves with desired speed magnitude v_α^0 in the positive x-direction. At $t_\alpha = 0.05$ s (upper left) the agent is oscillating around its desired direction. At $t_\alpha = 0.5$ s (upper right) the agent more smoothly moves toward its direction. At $t_\alpha = 1$ s and $t_\alpha = 5$ s (below left and right) the agent spirals around its goal.

The magnitude of $V_{\alpha\beta}^0$ determines how strong the agents are repelled by each other. The consequences of this term are explicitly shown in figure 3.9. In this situation, two agents head towards each other with a small y-offset and with desired direction towards the other side of the corridor. The simulations are in conformance with Johansson[32] and Qui et al.[6].

The consequences of the combination of boundary magnitude and interaction magnitude are illustrated in figure 3.10. The boundary magnitude $U_{\alpha B}^0$ determines how strongly the agents are repelled by any boundaries and, as discussed before, the interaction magnitude $V_{\alpha\beta}^0$ determines how strongly the agents are repelled by each other. When the boundary magnitude is set to the high value $U_{\alpha B}^0 = 100$ m^2/s^2 and the interaction magnitude to the low value $V_{\alpha\beta}^0 = 2.1$ m^2/s^2 the agents prefer to keep a larger distance from walls than from each other, as can be seen in the left of figure 3.10. Lane formation is not observed in this situation. In the middle figure 3.10 lane formation occurs. Here, due to the strong interaction potential $V_{\alpha\beta}^0 = 210$ m^2/s^2 it is more favourable for agents to walk in lanes in order to avoid collisions from oncoming agents. For $U_{\alpha B}^0 = 10$ m^2/s^2 and $V_{\alpha\beta}^0 = 2.1$ m^2/s^2 lane formation can be observed too, see the right of figure 3.10. Helbing and Mólnar use $U_{\alpha B}^0 = 10$ m^2/s^2 and $V_{\alpha\beta}^0 = 2.1$ m^2/s^2, [1]. However, the interaction magnitude $V_{\alpha\beta}^0 = 21$ m^2/s^2 is more in line with more recent literature, e.g. Qu et al. [6],Johansson et al. [32], and Ma et al. [33]. For this reason, the simulation model uses $V_{\alpha\beta}^0 = 21$ m^2/s^2.

DIRECTION

In Helbing and Mólnar's social force model only the part of obstacle B that is closest to agent α generates the repulsive effect $\vec{f}_{\alpha B}$, [1]. In section 2.3.7 it is concluded that the repulsive effect is always perpendicular to the inducing object.

In figure 3.11, the sum of the repulsive effect from boundary A (spanning (0.75, 2) to (2.5, 2)) and boundary

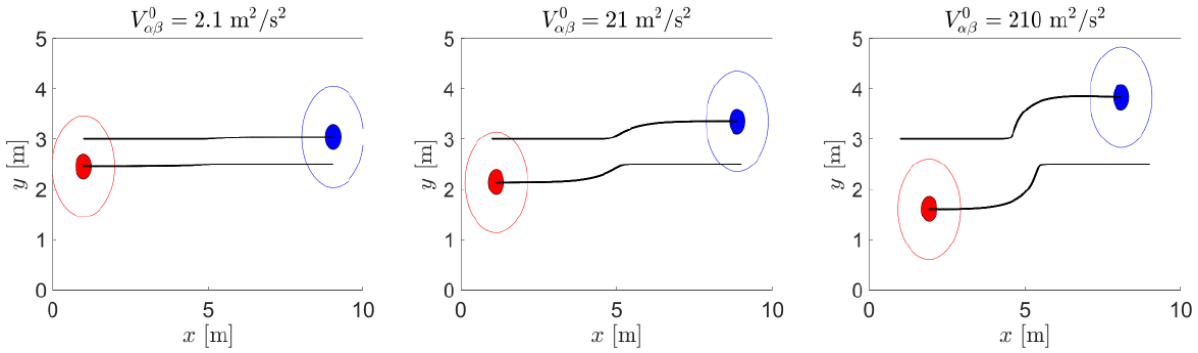

Figure 3.9: The strength of agent interaction repulsion depends on $V^0_{\alpha\beta}$. For stronger interaction magnitudes a larger repulsion can be observed.

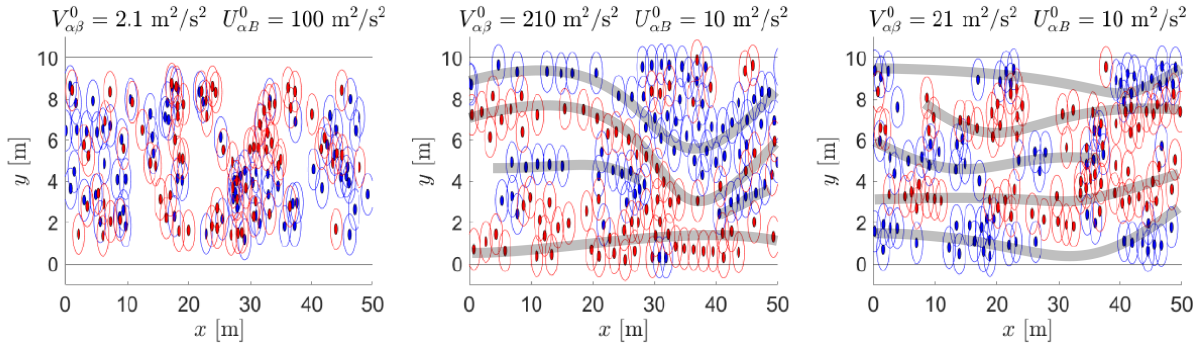

Figure 3.10: Agent distribution at $\#t = 5000$ iterations for varying $U^0_{\alpha B}$ and $V^0_{\alpha\beta}$. In the left figure agents prefer to keep larger distances to boundaries than to other agents, as a consequence of strong boundary potential and low interaction potential. In the middle and right figure lane formation is observed. Hollow circles (with radius 1 m) represent an agent's territorial space. The blue respectively red agents have a velocity towards the right respectively left side of the corridor. Lanes are indicated with a grey line.

B (spanning (2.5, 0.5) to (2.5, 2)) is illustrated for eight different agent positions. The most left agent, at coordinates (0.5, 1.5), feels no repulsion from boundary A as the agent is not located anywhere normal to this boundary. The agent's distance to boundary B is to large ($\geq$ 1 m) to show any significant effect. The second most left agent ((0.75, 1.5)) is just located normal to boundary A, and consequently feels a repulsive effect. However, boundary B is still to far away to generate any significant effect. Starting from $x = 1.75$ m, the repulsive effect generated by boundary B is becoming significantly stronger. Hence, the vector of the sum of both effects is pointing more and more to the left. The most right agent, at coordinates (2.25, 1.5) strongly feels a repulsion from boundary B and to a lesser extent by boundary A.

Please note that it is assumed that the edge of a boundary does not exert any effect as the boundaries are considered to have zero width.

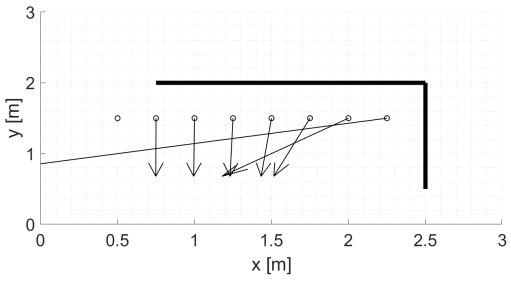

Figure 3.11: Agents at varying positions feel a different repulsive effect from boundary A (spanning (0.75, 2) to (2.5, 2)) and boundary B (spanning (2.5, 0.5) to (2.5, 2)).

SEMI-MINOR AXIS

Next to the interaction magnitude $V^0_{\alpha\beta}$, the interaction potential also depends on the semi-minor axis b, see equation 3.4.

$$V_{\alpha\beta} = V^0_{\alpha\beta} e^{-b/\sigma} \tag{3.4}$$

b is determined by both the distance $\|\vec{r}_{\alpha\beta}\|$ between agent α and agent β and the fact that other agents require space for their next step s_β:

$$2b = \sqrt{\left(\|\vec{r}_{\alpha\beta}\| + \|\vec{r}_{\alpha\beta} - \vec{v}_\beta \Delta t\|\right)^2 - \left(\vec{v}_\beta \Delta t\right)^2}. \tag{3.5}$$

The magnitude of $V_{\alpha\beta}$ mainly depends on the distance between agent α and agent β. This is illustrated in figure 3.12 and follows from the definition of b. By virtue of the walk over prevention, discussed in section 3.2.2, the distance between agent α and agent β will not become smaller than agent size $d_\alpha = 0.5$ m. In addition, the step size of agent β will not be larger than $s_\beta \approx 0.17$ m, as $s_{\beta max} = v^0_\beta v^{max}_{factor} \Delta t$ with $\langle v \rangle = 1.34$ m/s, $v^{max}_{factor} = 1.3$, and $\Delta t = 0.1$ s. Therefore, in most interactions s_β will be negligible when calculating b and $V_{\alpha\beta}$. However, the step size of agent β is still taken into account in the simulated model.

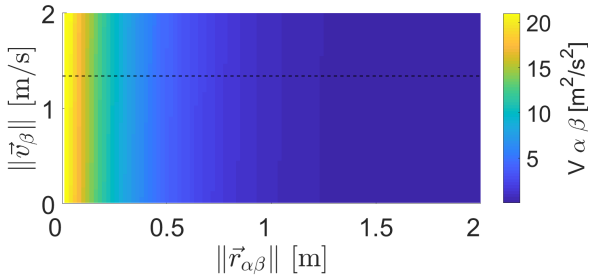

Figure 3.12: Dependence of interaction magnitude $V_{\alpha\beta}$ on the interagent distance $\|\vec{r}_{\alpha\beta}\|$ and velocity of agent β $\|\vec{v}_\beta\|$. $V_{\alpha\beta}$ mainly depends on $\|\vec{r}_{\alpha\beta}\|$. The average velocity $\langle v \rangle = 1.34$ m/s is indicated by the horizontal dashed line.

WALK OVER PREVENTION

In Helbing and Mólnar's [1] model agents are considered to be point particles. However, this approximation can result in so called walkovers. This is explained with reference to figure 3.13. Agents 2 and 3 are close to agent 1, resulting in an interaction effect $f_{2,3\to1}$ on agent 1 directed to the right. At the same time, agent 4 exerts an interaction effect $f_{4\to1}$ on agent 1 directed to the left. In this case, $f_{2,3\to1}$ has a bigger magnitude than $f_{4\to1}$ resulting in a nett interaction effect towards the right. If agent 4 does not move to the right far enough, agent 1 will walkover agent 4.

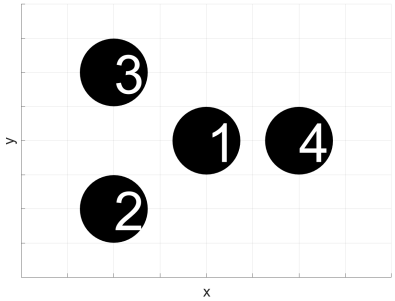

Figure 3.13: Agent 1 is pushed over agent 4 when the sum of the repulsion exerted by agents 2 and 3 is stronger than the repulsion from agent 4. This results in a walk over of agent 1 over agent 4.

In order to prevent these walkovers, agents are treated as particles with a hard kernel of agent size d_α. Based on average human metrics the agent size is set to $d_\alpha = 0.5$ m, [34]. Inside this hard core the interaction potential is theoretically infinite, as shown by the solid line in figure 3.14. However, two agents on a mutual distance $\|\vec{r}_{\alpha\beta}\| \leq d_\alpha$ would move to infinity due to such a potential, resulting in computationally impossible situations.

As a solution to walkovers, the actual velocity $\vec{v}_\alpha$ is set to zero when agent α is moving towards another agent β and their mutual distance $\|\vec{r}_{\alpha\beta}\|$ is smaller than or equal to agent size d_α, at iteration $\#t$. After that, the actual velocity will stay zero during the agents reaction time t_R, see equation 3.6. In this thesis' simulation the reaction time is set to 1.5 s.

$$\vec{v}_\alpha(\#t) = \begin{cases} \vec{0} & \|\vec{e}_\alpha \cdot \vec{r}_{\alpha\beta}(T)\| \leq d_\alpha \quad \text{with} T \in [\#t - t_R/\Delta t, \#t] \\ \vec{v}_\alpha(\#t) & \text{otherwise} \end{cases} \tag{3.6}$$

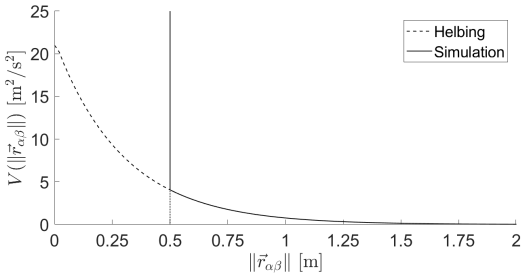

Figure 3.14: Interaction potential $V_{\alpha\beta}$ to inter-agent distance $\|\vec{r}_{\alpha\beta}\|$. The dashed line represents Helbing's interaction potential, the solid line represents a potential for agents with a hard core of diameter $d_\alpha = 0.5$ m.

The implementation of walkover prevention for a one dimensional path is shown in figure 3.15. In this figure agents with zero actual velocity $\vec{v}_\alpha$ are black, blue agents have a positive velocity directed to the right. At $\#t = 1$ agent 2 touches agent 3, activating the walk over prevention for $\#t = 2$. Subsequently, at $\#t = 2$ agent 2 is standing still. At $\#t = 3$, agent 1 touches agent 2, activating walk over prevention for agent 1 seen at $\#t = 4$.

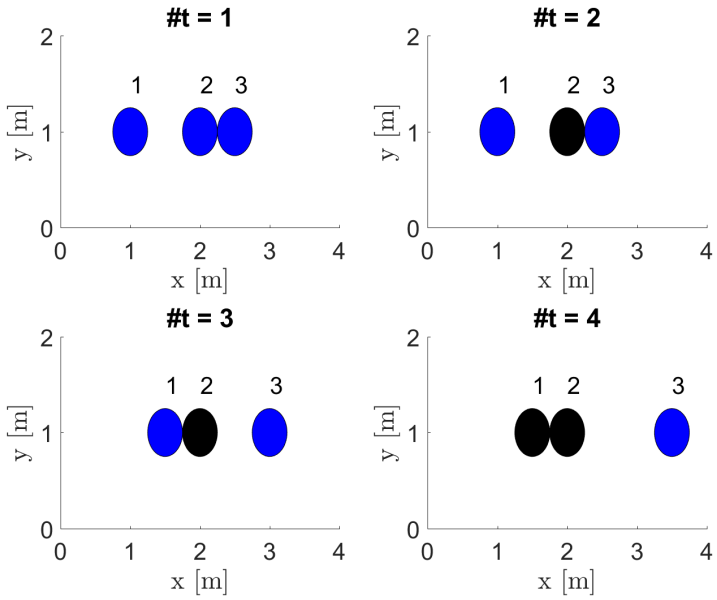

Figure 3.15: Walk over prevention for three agents moving to the right. Black agents are standing still, blue agents move to the right. After one agent touches another, the agent will not move any further due to walkover prevention.

GHOST PREVENTION

Similar to the effect causing walk overs, agents can get pushed through a wall at high interaction repulsions. To prevent this, another cut-off is implemented by which agents are stopped when the distance between agent α and boundary B is smaller or equal than the agent size: $\|\overrightarrow{r}_{\alpha B}\| \leq d_\alpha$. In contrast to walk over prevention, agents do not experience a reaction time here.

3.2.3. EFFECTS TO MOTION

From the sum of all effects $\vec{f}_\alpha(\#t)$ and the agent's previous actual velocity $\vec{v}_\alpha(\#t-1)$ the agent's new preferred velocity $\vec{w}_\alpha(\#t)$ is determined according to

$$\vec{w}_\alpha(\#t) = \vec{f}_\alpha(\#t)\Delta t + \vec{v}_\alpha(\#t-1). \tag{3.7}$$

If the magnitude of the preferred velocity is larger than the agent's maximum velocity v_α^{max}, the preferred velocity will be cut-off. With the unit-vector $\hat{w}_\alpha(\#t) = \vec{w}_\alpha(\#t)/\|\vec{w}_\alpha(\#t)\|$ this can be written as:

$$\vec{v}_\alpha(\#t) = \begin{cases} \vec{w}_\alpha(\#t) & \text{if } \|\vec{w}_\alpha(\#t)\| \leq v_\alpha^{max} \\ \hat{w}_\alpha(\#t)\, v_\alpha^{max} & \text{if } \|\vec{w}_\alpha(\#t)\| > v_\alpha^{max} \end{cases}. \tag{3.8}$$

Subsequently the agent's new position $\vec{r}_\alpha(\#t)$ is determined by

$$\vec{r}_\alpha(\#t) = \vec{v}_\alpha(\#t)\Delta t + \vec{r}_\alpha(\#t-1). \tag{3.9}$$

3.2.4. TELEPORT FUNCTIONALITY

By imposing a transversal periodic boundary condition it can be simulated that the agents walk in a circle shaped path. This stabilises any lane formation and other collective effects. On top of that, the length of the corridor can be treated as infinite, resulting in a boundary effect that is always perpendicular to the horizontal boundaries. The periodic boundary condition is acquired by a 'teleporting' function. When an agent reaches the corridor exit at either x_{min} or x_{max}, the agent is moved to the other exit and enters the corridor again. During this transition the agent's y-coordinate is conserved.

3.3. PROCESSING

3.3.1. CLUSTER ANALYSIS

To give a quantitative measurement for the number of lanes N_L, a cluster analysis method is developed for this thesis. This method is based on Hoogendoorn et al. [35], Sparnaaij [36], Ma et al.[33], and Zhang et al.[37].

According to Hoogendoorn et al., two agents form a cluster when they meet the conditions in equation 3.10. Hoogendoorn et al. does not give any values for the thresholds c_1 and c_2. However, Hoogendoorn et al. adds two interesting notes. First, at low agent densities relative much space is available between the agents. This can result in short lived patterns. Second, clusters are not per definition the same as lanes, and one lane can exist of multiple clusters.

$$\begin{cases} \|\vec{r}_\alpha - \vec{r}_\beta\| < c_1 \\ \|\vec{v}_\alpha - \vec{v}_\beta\| < c_2 \end{cases} \tag{3.10}$$

Regarding lane formation, Sparnaaij suggests to take into account the leader-follower relation, mentioning four conditions: 1) at least one follower, 2) every follower has approximately the same walking direction as the person in front of him, 3) every follower has approximately the same speed as the leader, and 4) an uninterrupted series of followers,[36]. These conditions form an extension on Hoogendoorn's conditions.

In the method developed for this thesis, agent α and agent β have to meet five criteria to form a cluster in a two dimensional corridor. First, their difference in x-position has to be lower or equal than $r_{max,\,x} = 10$ m. Hence, agents are allowed to keep a certain maximum distance to their leader. Second, the difference in y-position is not allowed to exceed the average agent size $r_{max,\,y} = 0.5$ m. By this criteria, agents that move side by side without following can not form a cluster. The third criteria requires the agents to have approximately the same velocity. Their velocities can differ by maximal 1 m/s. Fourth, the agents have to move in approximately the same direction. Here, the maximal direction difference is set to $e_{max} = 20°$. For the final criteria, agent β should be in a certain angle of sight of agent α. For this, an axial system centred at agent α ($\vec{r}_\alpha$) and with the axis A parallel with agent α's direction ($\vec{e}_\alpha$) is taken, see figure 3.16. Then, the angular position θ_β of agent β relative to axis A has to be lower than or equal to the maximum angle of sight $\phi_{max} = 20°$.

1. $|r_{\alpha,\,x} - r_{\beta,\,x}| \leq r_{max,\,x}$
2. $|r_{\alpha,\,y} - r_{\beta,\,y}| \leq r_{max,\,y}$

3. $\|\vec{v}_\alpha - \vec{v}_\beta\| \leq v_{max}$
4. $\|\vec{e}_\alpha - \vec{e}_\beta\| \leq e_{max}$
5. $\theta_\beta \leq \phi_{max}$

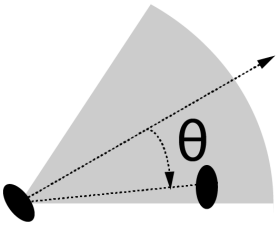

Figure 3.16: Agent β is in the vision of agent α when its angular position (θ_β) relative to the direction of agent α ($\vec{e}_\alpha$) meets $\theta_\beta \leq \phi_{max}$.

The cluster analysis method is illustrated in figure 3.17. In the left of the figure $r_{max,\,y} = 0.5$ m and right $r_{max,\,y} = 5$ m. All other thresholds are equal for both images, namely $r_{max,\,x} = 10$ m, $v_{max} = 1$ m, $e_{max} = 20°$, and $\phi_{max} = 20°$ and the agent distribution is the same. An increase in $r_{max,\,y}$ increases the number of clusters. A similar effect occurs for other threshold values.

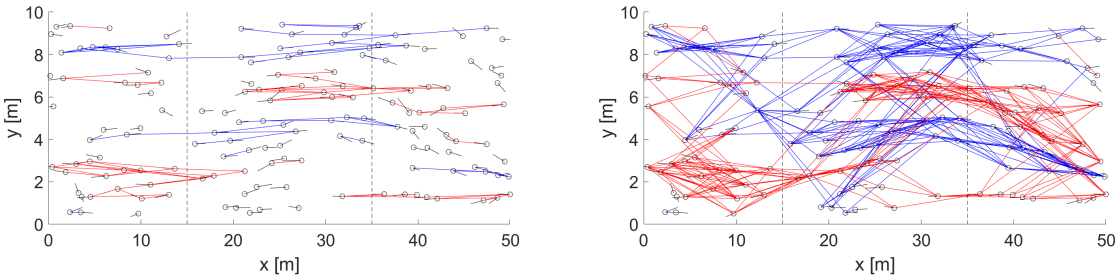

Figure 3.17: Clusters for $r_{max,\,y} = 0.5$ m (left) and $r_{max,\,y} = 0.5$ m (right). An increase in $r_{max,\,y}$ strongly increases the number of clusters. The blue respectively red lines connect clusters of agents moving to the right, respectively to the left. Circles represent agents, the small black lines show the agents' actual velocity. The cluster area spans from $x = 15$ m to $x = 35$ m. Both images have the same agent distributions.

Subsequently, an indication for the number of lanes N_L is acquired by averaging the number of counted clusters N_C over time, according to equation 3.11. Only clusters in the cluster area spanned by $x = W_C$ and corridor width $y = Y$ are counted, as shown by the dashed lines in figure 3.17.

$$\overline{N_C} = \frac{1}{T} \sum_{\#t \in T} N_C(\#t) \tag{3.11}$$

Figure 3.18 shows that $\overline{N_C}$ increases with cluster area width W_C. After all, an increase in cluster area causes an increase in the number of clusters *in* that area. A condition for the cluster analysis method to work is $\overline{N_C} \propto W_C$. Figure 3.19 shows $\overline{N_C} \propto W_C$ approximately holds in the domain $W_C \in [10,\ 30]$ m. Therefore, it is important to maintain a constant value $W_C \in [10,\ 30]$ m. In this thesis $W_C = 20$ m.

3.3.2. AVERAGE VELOCITY AND FLOW

The average velocity is defined as the sum of the absolute velocity in the x-direction for all agents α for all iterations $\#t \in T$, divided by the product of the total number of agents N_α times T, as given by equation 3.12. As the simulation is stable after approximately 1000 iterations, $\#t$ has to be larger or equal to 1000. In this thesis $\$t \in [1500, 2000]$.

$$\overline{v} = \frac{1}{T N_\alpha} \sum_{\#t \in T} \sum_{\alpha \in N_\alpha} |v_\alpha^x(\#t)| \tag{3.12}$$

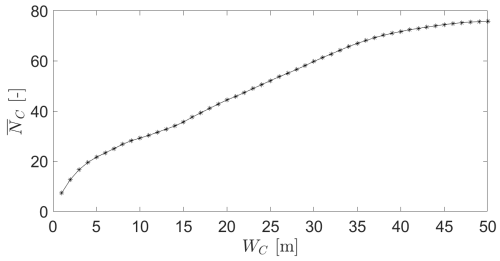

Figure 3.18: The average number of counted clusters $\overline{N_C}$ increases with W_C, the width of the area in which the clusters are counted.

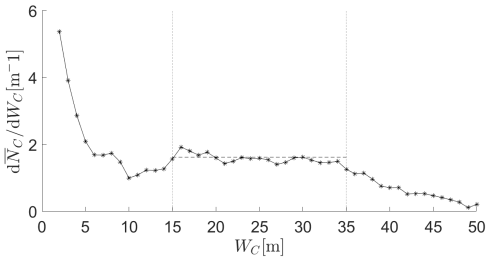

Figure 3.19: $\overline{N_C}$ differntiated to W_C. In $W_C \in [10, 30]$ m the number of counted clusters $\overline{N_C}$ increases approximately linearly with cluster width W_C.

Subsequently, for one dimensional situations like Seyfried et al.'s experiment the flow J is calculated using the agent line density λ and the average velocity $\overline{v}$ according to equation 3.13.

$$J = \lambda \overline{v} \tag{3.13}$$

4

VALIDATION

4.1. FUNDAMENTAL DIAGRAM

Seyfried et al. precisely describe an empiric experiment to determine the average velocity for different pedestrian densities, [2]. By mimicking this experiment the interaction effect and walk over prevention of the simulation model are quantitatively validated.

EXPERIMENTAL SET-UP

Seyfried et al.[2] describe a set up with a circular passageway as in figure 4.1. All pedestrians walk in one line and obey unidirectional flow. The set up is considered to be one dimensional. The passageway is described to have a total length of $X = 17.3$ m and a width of $Y = 0.8$ m. This width prevents any overtaking and is assumed not to induce any repulsive boundary effects. The set up is built by chairs and ropes. By virtue of its circular shape the corridor has periodic boundary conditions. The test subjects are instructed not to overtake and not to hurry. The number of test subjects in the passageway is varied in order to change the density. In Seyfried et al. the local density and velocity in a specific area of 2 m length is determined. In the simulated model the density and velocity are determined over the whole path length, according to equation 3.12. Subsequently, for both Seyfried et al. and the simulation the flow J is calculated according to equation 3.13.

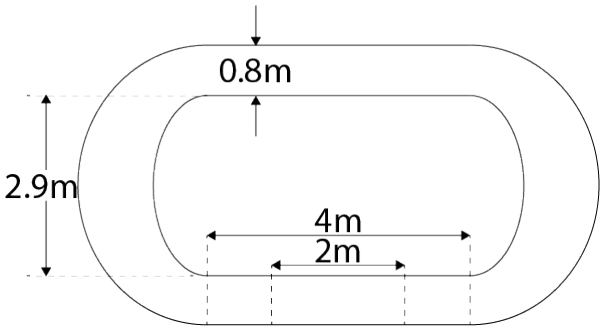

Figure 4.1: Experimental set-up as described by Seyfried et al., [2]. Pedestrians walk in one line obeying unidirectional flow without overtaking. The pedestrians follow a circular path of total length $X = 17.3$ m.

OBTAINED DATA

For $\lambda \in [0.5,\ 1.5]$ m^{-1}, the obtained data are in good agreement with the data found by Seyfried et al., see figure 4.2. For $\lambda \in (1.5,\ 2]$ m^{-1} Seyfried et al. found velocities that *do not* go to zero. This is not in accordance with most prevailing studies, including [38], [39], [40], and [41], where the velocities *do* go to zero. The simulated data does resemble these other studies. Interestingly, this finding causes Seyfried et al. to suggest to revisit the prevailing fundamental diagram.

REACTION TIME

In the simulation of Seyfried et al.'s experiment, a reaction time $t_R = 1.5$ s is used, see section 3.2.2. Higher reaction times result in lower average velocities but show a similar shape, as shown in figure 4.3.

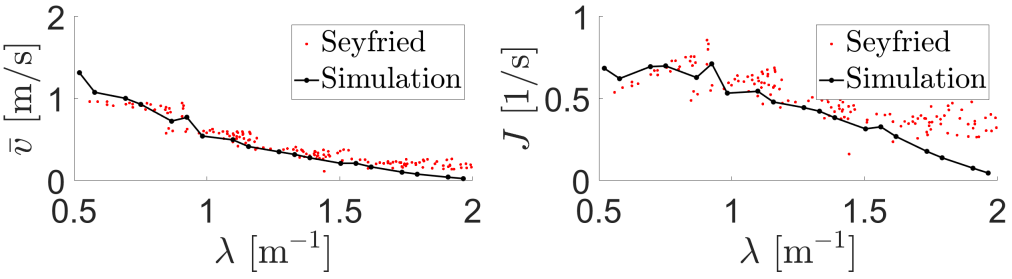

Figure 4.2: Fundamental diagram for a one-dimensional corridor. Seyfried et al.'s [2] empirical data (red) and the simulated data (black) show strong resemblances. Left: average velocity for different pedestrian line densities. Right: pedestrian flow for different pedestrian line densities. Please note that the flow is calculated directly from the average velocity $\overline{v}$.

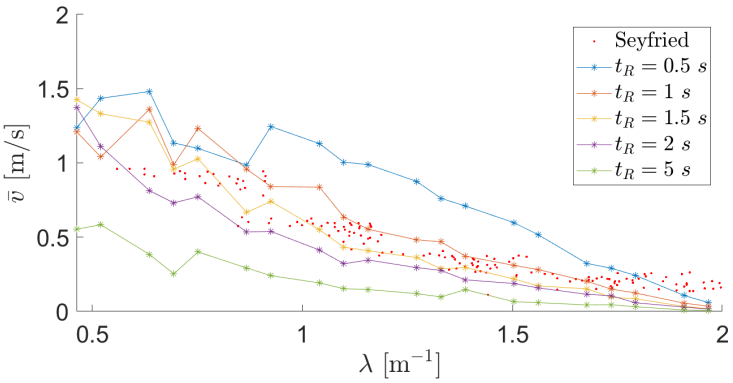

Figure 4.3: Fundamental diagram for a one-dimensional corridor. Seyfried et al.'s [2] empirical data (red dots) and simulated data for varying reaction times t_R.

4.2. LANE FORMATION

When introducing their social force model, Helbing and Mólnar[1] showed a linear relation between the number of lanes and the width of the corridor. The simulation model has a similar linear relation, resulting in a qualitative validation. However, due to an unknown lane definition, a quantitative comparison with Helbing and Mólnar is not possible.

EXPERIMENTAL SET-UP

Helbing and Mólnar describe a computer simulation in which agents walk through a corridor. In their article the average number of lanes $\overline{N_C}(Y)$ is counted for corridor widths Y varying between 2 and 20 m, [1]. Helbing and Mólnar use interaction magnitude $V^0_{\alpha\beta} = 2.1\text{m}^2/\text{s}^2$ and time step $\Delta t = 2$ s, [1]. However, the simulated model uses $V^0_{\alpha\beta} = 21\text{m}^2/\text{s}^2$ and $\Delta t = 0.1$ s, for reasons discussed in section 3.2.2. All other parameters are set equal to the values used by Helbing and Mólnar, as noted in the Nomenclature.

CLUSTER ANALYSIS METHOD

Helbing and Mólnar do not give a clear definition of a lane, as follows from an example with caption: "Here the computational result shows N = 4 (or 5) lanes", [1, p. 4285]. For a quantitative measure of the number of lanes, the cluster analysis method described in section 3.3.1 is used.

OBSERVED DATA

The average number of clusters $\overline{N_C}$ in the simulation and the average number of lanes $\overline{N_L}$ found by Helbing and Mólnar are shown in figure 4.4. Both data show a linear relation of the number of clusters/lanes with corridor width Y. Due to differences in definition the data vary in slope and offset. Helbing and Mólnar find the linear relation $\overline{N_L}(Y) = 0.36\text{m}^{-1}Y + 0.59$, [1]. The simulated data has the linear relation $\overline{N_C}(Y) = 4.4\text{m}^{-1}Y - 1.1$.

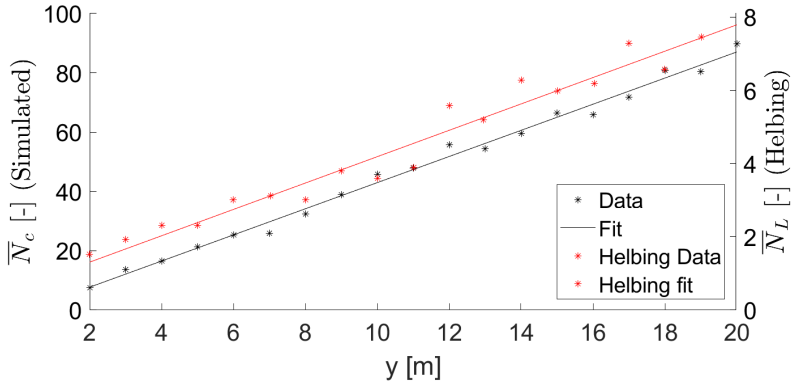

Figure 4.4: Number of simulated clusters $\overline{N_C}$ (black) and Helbing and Mólnar's [1] found number of lanes $\overline{N_L}$ (red) for varying corridor widths Y. Both the simulated data as the data found by Helbing and Mólnar show a linear increase with Y. Please note that the right axis is knowingly adjusted to suggest a corresponding slope.

LINEAR RELATION: TRIVIAL?

On first sight, an increase of the number of lanes N_L with corridor width Y might seem trivial. After all, a wider corridor gives space for more agents to walk side by side, subsequently forming more lanes. Using a reductio ad impossibilem it will be shown that this relation is not trivial. First assume that the number of lanes N_L only depends directly on the corridor width Y. It is explicitly stated that in this assumption the number of lanes does not depend on any attractive or repulsive effects. In this assumption, the number of lanes would be determined directly by the amount of agents that fit next to each other in the corridor, shoulder to shoulder. As the agents have a width $d_\alpha = 0.5$ m, the number of lanes would be determined by $N_L = 1/d_\alpha Y = 2Y$, without any offset. However, Helbing and Mólnar do find a relation with a very different slope and with an offset, namely $N_L(Y) = 0.36\text{m}^{-1}Y + 0.59$, [1]. From this it is concluded that the first assumption is not correct. Therefore, the linear relation is not trivial.

4.3. NARROW DOOR

Collective effects observed in the simulation model show resemblances with computer simulations done by Helbing and Mólnar, [1]. This qualitatively validates the correct simulation of the driving, boundary and interaction effect.

EXPERIMENTAL SET-UP

The addition of two walls with a small door-like opening creates another experimental set-up. This experiment is done by Helbing and Mólnar, [1]. The obstacles are situated halfway the corridor, at $x = 25$ m. The width of the opening is set to $W_d = 1$ m, and is situated in the middle of the corridor, at $y = 5$ m. Initially, all agents with a desired direction towards the right are randomly distributed on the left of the obstacle. Agents with a desired direction towards the left are randomly distributed on the right side. The initial situation of the simulation model is shown in the left of figure 4.5.

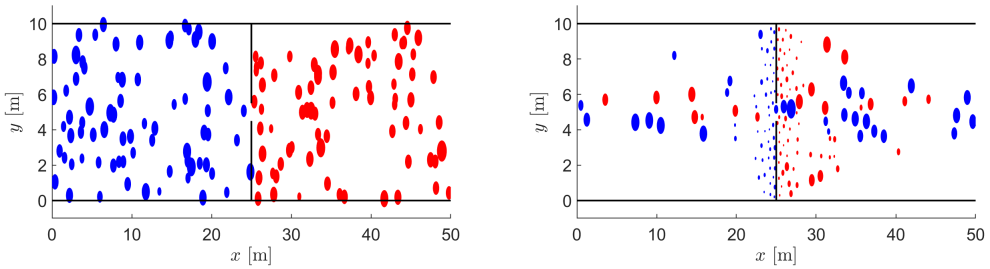

Figure 4.5: Agents passing through a door. Left: initial distribution. Right: distribution after $\#t = 3000$ iterations. Agents follow the path of their predecessor. Agents moving to the right respectively left are coloured blue respectively red, the size of a circle represents the agent's velocity.

OBSERVED PHENOMENA

The agents move in their desired direction, until they are stopped by an obstacle or by another agent. Only 1 to 2 agents can move through the opening at the same time, resulting in a bottleneck. Once one agent manages to pass through the opening, others follow in his path. This can be seen in both the simulation in the right of figure 4.5 and in Helbing and Mólnar's [1] result shown in figure 4.6.

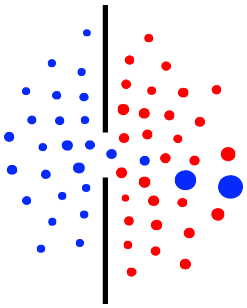

Figure 4.6: Agents passing through a door, as redrawn from Helbing and Mólnar, [1]. Agents moving to the right respectively left are coloured blue respectively red, the size of a circle represents the agent's velocity. Once on agent manages to pass the door, others follow.

5

CONCLUSIONS AND DISCUSSION

To investigate the underlying thought of the social force model, this work attempts to answer the following question:

"What are the physical consequences of the effects and parameters of the social force model?"

This question is answered by implementing the social force model. An overview of all conclusions is given in this chapter. In addition, made assumptions and suggestions for further research are discussed.

5.1. ADJUSTMENTS TO THE SOCIAL FORCE MODEL

5.1.1. HARD KERNEL AGENTS

Contrary to Helbing and Mólnar's [1] model, the model of this thesis treats agents as particles with a hard kernel in order to prevent agents from walking over each other or walking through boundaries. As it is computationally unwise to use infinite potentials, a specific walkover prevention and ghost prevention functionality are created.

Both the walkover prevention and ghost prevention functionality result in a sudden change of movement. For a more smooth behaviour the functionalities can be replaced by a potential $U(r)$ of the form

$$U(r) = A_1 e^{-r/c_1} + A_2 e^{-r/c_2} \tag{5.1}$$

With r the distance between the agent and another repulsive object. By setting $A_1 \ll A_2$ and $c_1 \gg c_2$ the second term overrules the first for very small distances only, resulting in a far stronger potential close to the repulsive object. This allows for a continuous potential becoming very high but finite.

WALKOVER PREVENTION AND REACTION TIME

When agent α walks into another agent at time $t_{collision}$, its actual velocity $\vec{v}_\alpha(t)$ is set to zero for $t \in [t_{collision}, t_{collision} + t_R]$, with $t_R = 1.5$ s the reaction time of agent α. The value of t_R has a strong impact on the overall average velocity $\overline{v}$. Human reaction times vary strongly, from under 0.5 s for expected events to 1.5 s for unexpected events, [42], [43]. The value of t_R is based on a quick computational analysis, but not validated by empirical research. $t_R = 1.5$ s is probably on the high side, and has to be investigated in further research.

GHOST PREVENTION

The ghost prevention functionality moves an agent away from a boundary as soon as it tends to walk through this boundary. Unlike the walkover prevention, the agent can directly continue its movement after a collision with a boundary. Here, the agent is considered to have a reaction time $t_R = 0$ s, because the boundary collision is seen as an expected event.

5.1.2. INTERACTION MAGNITUDE

Helbing and Mólnar [1] suggest an interaction magnitude $V^0_{\alpha\beta} = 2.1$ m^2/s^2. However, for this value lane formation is barely visible in the developed simulation model of this thesis. More recent studies suggest an interaction magnitude $V^0_{\alpha\beta} \sim 2 \cdot 10$ m^2/s^2, e.g. [6],[32], and [33]. Therefore, this thesis uses $V^0_{\alpha\beta} = 21$ m^2/s^2. However, it has to be noted that no reason exists to specifically choose 21 m^2/s^2 over any other value of the same magnitude.

5.1.3. ITERATION TIME STEP

A too high value of iteration time step Δt can result in overshooting behaviour, as a small effect results in a large difference in position. After a computational analysis it is decided to use $\Delta t = 0.1$ s.

A iteration time step $\Delta t = 0.1$ s implies that a pedestrian re-evaluates his motion every 0.1 s. This appears not to be in line with the earlier mentioned slow reaction time $t_R = 1.5$. On the contrary, other more recent simulations use even smaller values, e.g. $\Delta t = 0.01$ s, [6], and $\Delta t = 0.05$ s, [31].

5.2. WORKING OF THE SOCIAL FORCE MODEL

5.2.1. BOUNDARY AND INTERACTION EFFECT

Both the boundary and interaction effect repel the agent away from the generating object, with a magnitude that decreases with distance $\|\vec{r}_{\alpha j}\|$ according to the general form:

$$\vec{f} = -\nabla_{\vec{r}_{\alpha j}} A e^{-\|\vec{r}_{\alpha j}\|/c}.$$

5.2.2. PARAMETERS

Four noteworthy parameters are the relaxation time t_α, velocity distribution $\sqrt{\theta}$, agent density ρ, and agent line density λ. The relaxation time is a measure for the aggressiveness of agent α and has the value $t_\alpha = 0.5$ s. For lower values the agent becomes more aggressive and shows a more sharp-edged motion. The velocity distribution determines how strong the agents' desired velocities differ, in most cases set to $\sqrt{\theta} \sim 0.3$ m/s. For a high velocity distribution ($\sqrt{\theta} \sim 1$ m/s) the agents' magnitudes of desired velocity differ strongly and jamming occurs. Unless otherwise specified the agent density is set to $\rho \sim 0.3$ pedestrian m^{-2}, and agent line density $\lambda = 0.1 \sim 2$ pedestrian m^{-1}. These two parameters can impact jamming. The simulation shows that at high pedestrian densities $\lambda \geq 1.5$ pedestrians m^{-1} the average velocity $\overline{v}$ goes to zero.

5.2.3. ASSUMPTIONS

DECISION MAKING BASED ON EFFECTS

One of the fundamentals of the social force model is the assumption that social force effects have a direct influence on the motion of pedestrians. Although many empirical studies have proven the power of the social force model, these studies do not always make a connection between human psychological principles and collective effects. For further research and a better understanding it is recommended to investigate more in this connection, [44].

KNOWLEDGE ABOUT ENVIRONMENTS

The use of the driving effect as defined by Helbing and Mólnar [1] assumes that pedestrians always know their destination. In addition, agents always take the shortest route in stead of the fastest route. This is not always conform realistic situations. To solve this, 'in-between'-goals can be implemented, to guide an agent through a more irregular path. However, these 'in-between'-goals strongly influence the total outcome, so require good empirical studies.

NEGLECTING ATTRACTIVE EFFECTS

The simulations done by Helbing and Mólnar [1] neglect any attractive effects. While a plain corridor does indeed lack any attractive objects like windows or paintings, some agents might get attracted by others. Therefore, the use of attractive effects contributes to more realistic simulations.

AGENTS ARE TREATED AS CIRCLES

In the simulations the agents are treated as particles with a circular circumference. Although most humans prefer to keep a larger distance from their face than from their sides, a circular approximation can be to blunt, especially in highly crowded situations.

BOUNDARY SIZES

The boundary effects assumes every boundary to have infinite length and zero depth. This approximation is valid for the corridor walls that span in the x-direction, by virtue of the transversal periodic boundary conditions. However, this approximation is not correct for the narrow door situation. Here pedestrians would feel a repulsion by the tips of the boundaries that enclose the door. Taking this into account, passing through the door would be more difficult.

INITIAL VELOCITY AND DISTRIBUTION

In Helbing and Mólnar [1] agents enter the corridor at the start of the simulation. In the simulated model all agents start randomly distributed inside the corridor. In addition, the agents start the simulation with their desired velocity directed towards their destination. However, by virtue of the converging characteristics this difference in initial distribution is regarded to have no impact on the outcome of the simulation.

5.3. VALIDATION

5.3.1. FUNDAMENTAL DIAGRAM

The simulated fundamental diagram for a one-dimensional case is in good resemblance with the prevalent observations, offering a quantitative validation. The simulated data show strong similarities with the empirical experiment done by Seyfried et al.[2] for pedestrian line densities $\lambda \in [0.5,\ 1.5]$ m^{-1}. For $\lambda \in (1.5,\ 2]$ m^{-1} the obtained data varies from Seyfried et al.'s results. However, here Seyfried et al.'s observations differ from the prevalent studies while the computer simulations are still compliant with these studies, e.g. [38], [39], [40] and [41].

Despite the good results, it has to be noted that a relation between velocity and pedestrian density is not yet tested for a two dimensional case. For a good result the walkover prevention functionality needs some adjustments, as the current version is focused on movement in the x-direction only. Another point of remark is the importance of reaction time t_R. Values of $t_R \neq 1.5$ s do show a decrease in average velocity for higher densities too, but have a slope that differs from Seyfried et al.'s results.

5.3.2. LANE FORMATION

A qualitative validation is given by the observed linear relationship between the average number of clusters $\overline{N_C}$ and corridor width Y. This linearity is in agreement with Helbing and Mólnar's[1] data. However, due to differences in definition the slope and offset of the retrieved relationship cannot quantitatively be compared with Helbing and Mólnar's results. A cluster analysis method is developed to give an indication for the number of lanes. Please see section 5.4 for critical notes on this topic.

5.3.3. NARROW DOOR

Collective effects observed in the simulation model show resemblances with computer simulations done by Helbing and Mólnar, [1]. This qualitatively validates the correct simulation of the driving, boundary and interaction effect.

5.4. CLUSTER ANALYSIS METHOD

For a quantitative measure of the number of lanes N_L a cluster analysis method is developed. Following this method, agent α and agent β have to meet the following five criteria:

1. $|r_{\alpha,\,x} - r_{\beta,\,x}| \leq r_{max,x} = 10$ m,
2. $|r_{\alpha,\,y} - r_{\beta,\,y}| \leq r_{max,y} = 0.5$ m,
3. $\|\vec{v}_\alpha - \vec{v}_\beta\| \leq v_{max} = 1$ m/s,
4. $\|\vec{e}_\alpha - \vec{e}_\beta\| \leq e_{max} = 20°$, and
5. $\theta_\beta \leq \phi_{max} = 20°$.

Three remarks need to be made about these conditions. First, the threshold values are not validated to any (empirical) studies but based on a computational analysis. In further research these values have to be validated and possibly adjusted. Second, the thresholds $r_{max,\,x}$ and $r_{max,\,y}$ apply for uni- and bidirectional flow in the x-direction only. For a more generic method it is advised to replace the first two conditions by

1. $|\vec{r}_\alpha \cdot \vec{e}_{\alpha,\parallel} - \vec{r}_\beta \cdot \vec{e}_{\alpha,\parallel}| \leq r_{max,\parallel} = 10$ m,
2. $|\vec{r}_\alpha \cdot \vec{e}_{\alpha,\perp} - \vec{r}_\beta \cdot \vec{e}_{\alpha,\perp}| \leq r_{max,\perp} = 0.5$ m.

Where $\vec{e}_{\alpha,\parallel}$ respectively $\vec{e}_{\alpha,\perp}$ represent the unit vector parallel respectively perpendicular to the direction of agent α.

As final remark about the cluster analysis method, the current method does not take into account Sparnaaij's suggestion that the agents have to form a uninterrupted lane, [36]. This can be solved by defining $r_{\alpha j,\parallel} = |\vec{r}_\alpha \cdot \vec{e}_{\alpha,\parallel} - \vec{r}_j \cdot \vec{e}_{\alpha,\parallel}|$ and adding the following condition:

- $\min_j |r_{\alpha j,\parallel}| = |r_{\alpha\beta,\parallel}|$.

Next to these specific conditions, two more remarks are made about this method. First of all, in the current method every single agent combination is counted as one cluster. This is appropriate when solely used as indication for the number of lanes. However, when only the amount of 'complete clusters' is counted the result is more likely to meet the actual number of lanes. This can be implemented by a computational trick.

Furthermore, the relation $\overline{N_C} \propto W_C$ does not hold for every cluster width W_C. It is important to stay aware of this problem and keep a constant value of W_C when future comparisons are made. (In this thesis $W_C = 20$ m.) A more accurate definition of a cluster can help in solving this problem.

5.5. FURTHER RESEARCH

More than anything else, quantitative investigations in parameter values are required. The social force model is a well known and established model but its applicability strongly depends on the values of its parameters, [44]. In addition, every specific simulated situation can require its own parameter values, [7], [45]. Next to this, the effect of cultural specific characteristics on parameter values needs further investigation, [46]. For the validation of these parameters concrete and quantifiable definitions are needed, [47]. However, these definitions do not yet exist, [48].

Via the cluster analysis model this thesis made a small attempt to come any closer to a quantifiable definition of lane formation, building on suggestions by Hoogendoorn et al. [35] and Sparnaaij [36]. However, this method requires more investigations and empirical validation.

Next to this, the adjusted social force model can easily be extended with unique agent characteristics, e.g. a relaxation term t_α that varies per agent. Such a refinement contributes to the model's ability to generate future realistic simulations.

BIBLIOGRAPHY

[1] D. Helbing and P. Molnár. Social force model for pedestrian dynamics. *Physical Review E*, 51:4282–4286, 1995.

[2] A. Seyfried, B. Steffen, W. Klingsch, and M. Boltes. The fundamental diagram of pedestrian movement revisited. *Journal of Statistical Mechanics: Theory and Experiment*, 2005(10):P10002, 2005.

[3] P. Faigle, dpa, Reuters, P. Sadigh, and M. Horeld. Fragen und antworten zum unglück. *Zeit Online*, 2010.

[4] X. Zheng, T. Zhong, and M. Liu. Modeling crowd evacuation of a building based on seven methodological approaches. *Building and Environment*, 44:437–445, 2009.

[5] X. Chen, M. Treiber, V. Kanagaraj, and H. Li. Social force models for pedestrian traffic – state of the art. *Transport Reviews*, 38(5):625–653, 2017.

[6] Y. Qu, Y. Xiao, J. Wu, T. Tang, and Z. Gao. Modeling detour behavior of pedestrian dynamics under different conditions. *Physica A*, 492:1153–1167, 2018.

[7] M. Sparnaaij. How to calibrate a pedestrian simulation model. Msc thesis, 09 2018.

[8] A. Templeton, J. Drury, and A. Philippides. From mindless masses to small groups: Conceptualizing collective behavior in crowd modeling. *Review of General Psychology*, 19:215–229, 2015.

[9] H. Klüpfel. Crowd dynamics phenomena, methodology, and simulation. In *Pedestrian Behavior*. Emerald Group Publishing Limited, 2009.

[10] A Schadschneider, W Klingsch, H Klüpfel, T Kretz, C Rogsch, and A Seyfried. Evacuation dynamics: Empirical results, modeling and applications. In *Encyclopedia of Complexity and Systems Science*, pages 517–550. Springer New York, 2011.

[11] J.J Fruin. *The Causes and Prevention of Crowd Disasters.* Elsevier Science Publishers B.B., 2002.

[12] D.C. Duives. Analysis of pedestrian crowd movements at lowland. MSc thesis, 2012.

[13] G.H. Goldsztein. Particles moving around a two-lane circular track in both directions; avoiding collisions leads to self-organization. *Society for Industrial and Applied Mathematics*, 76:1433–1445, 2016.

[14] N.R. Johnson. Panic at "the who concert stampede": An empirical assessment. *Social Problems*, 34:362–373, 1987.

[15] P.A. Thompson and E.W. Marchant. Simulex; developing new computer modelling techniques for evaluation. *Fire Safety Science – 4th international Symposium Proceedings*, 4:613–624, 1994.

[16] N. Bellomo and A. Bellouquid. On multiscale models of pedestrian crowds from mesoscopic to macroscopic. *Communications in Mathematical Sciences*, 13:1649–1664, 2015.

[17] A. Kirchner, K. Nishinari, and A. Schadschneider. Friction effects and clogging in a cellular automaton model for pedestrian dynamics. *Physical Review*, 67:056122, 2003.

[18] W.F. Fang, L.Z. Yang, and W.C. Fan. Simulation of bi-direction pedestrian movement using a cellular automata model. *Physica A*, 321:633–640, 2003.

[19] K. Nishinari, K. Sugawara, T. Kazama, and A. Schadschneider. Modelling of self-driven particles: foraging ants and pedestrians. *Physica A*, 372:132–141, 2003.

[20] L.Z. Yang, D.L. Zhao, J. Li, and T.Y. Fang. Simulation of the kin behavior in building occupant evacuation based on cellular automaton. *Building and Environment*, 40:411–415, 2005.

[21] K. Yamamoto, S. Kokubo, and K. Nishinari. Simulation for pedestrian dynamics by real-coded cellular automata (rca). *Physica A*, 379:654–660, 2007.

[22] D. Helbing, I.J. Farkas, P. Molnár, and T. Vicsek. Simulation of pedestrian crowds in normal and evacuation situations. *Pedestrian and evacuation dynamics*, 21:21–58, 2002.

[23] R.L. Hughes. The flow of human crowds. *Annual Review of Fluid Mechanics*, 35:169–182, 2003.

[24] A. Braun, Bodmann B.E.J., and S.R. Musse. Simulating virtual crowds in emergency situations. In *Proceedings of the ACM Symposium on Virtual Reality Software and Technology*, pages 244–252, New York, NY, USA, 2005. ACM.

[25] M.C. Toyama, A.L.C. Bazzan, and R. Da Silva. An agent-based simulation of pedestrian dynamics: from lane formation to auditorium evacuation. In *Proceedings of the Fifth International Joint Conference on Autonomous Agents and Multiagent Systems*, pages 108–110. ACM, New York, USA, 2006.

[26] E. Bonabeau. Agent-based modeling: Methods and techniques for simulating human systems. *Proceedings of the National Academy of Sciences*, 99(3):7280–7287, 2002.

[27] D. Helbing, A. Johansson, W. Yu, M. Moussaid, I. Farkas, P. Molnar, and T. Vicsek. Pedestrian, crowd, and evacuation dynamics. University Lecture ETH Zürich, 06 2016.

[28] R.Y. Guo and H.J. Huang. A mobile lattice gas model for simulating pedestrian evacuation. *Physica A*, 387:580–586, 2008.

[29] W.G. Song, X. Xu, B.H. Wang, and S.J. Ni. Simulation of evacuation processes using a multi-grid model for pedestrian dynamics. *Physica A*, 363:492–500, 2006.

[30] D.R. Parisi, S.A. Soria, and R. Josens. Faster-is-slower effect in escaping ants revisited: Ants do not behave like humans. *Safety Science*, 72:274 – 282, 2015.

[31] F. Johansson, D. Duives, W. Daamen, and S. Hoogendoorn. The many roles of the relaxation time parameter in force based models of pedestrian dynamics. *Transportation Research Procedia*, 2:300–308, 2015.

[32] A. Johansson. Bi-directional flow in the social force model. Bsc. thesis, 2016.

[33] J. Ma and W. Song. Automatic clustering method of abnormal crowd flow pattern detection. *Procedia Engineering*, 62:509–518.

[34] C.D. Fryar, Q. Gu, and C.L. Ogden. Anthropometric reference data for children and adults: United states, 2007–2010. *Vital Health Stat*, 11, 2012.

[35] S Hoogendoorn and W. Daamen. Self-organization in walker experiments. In *Proceedings of the 5th Symposium on Traffic and Granular Flow*. 01 2004.

[36] M. Sparnaaij. Private communication, 06 2018.

[37] J. Zhang, W. Klinsch, A. Schadschneider, and A. Seyfried. Ordering in bidirectional pedestrian flows and its influence on the fundamental diagram. *Journal of Statistical Mechanics: Theory and Experiment*, 2012:P02002, 2012.

[38] U. Weidmann. *Transporttechnik der Fussgänger*. Schriftenreihe des IVT, ETH Zürich, 1993.

[39] D. Helbing, A. Johansson, and H.Z. Al-Abideen. Dynamics of crowd disasters: An empirical study. *Physical Review E*, 75:046109–1 – 046109–7, 2007.

[40] B.D. Hankin and R.A. Wright. Passenger flow in subways. *Operational Research Society*, 9:81–88, 1958.

[41] V.J. Blue and J.L. Adler. Cellular automata microsimulation for modeling bi-directional pedestrian walkways. *Transportation Research Part B*, pages 293 –312.

[42] H. Summala. Brake reaction times and driver behavior analysis. *Transportation Human Factors*, 2:217 – 226, 2000.

[43] A. Jain, R. Bansal, A. Kumar, and K.D. Singh. A comparative study of visual and auditory reaction times on the basis of gender and physical activity levels of medical first year students. *International Journal of Applied and Basic Medical Research*, 5:124–127, 2015.

[44] P. Wang. Understanding Social-Force Model in Psychological Principles of Collective Behavior. *ArXiv e-prints*, May 2016.

[45] M. Campanella. *Microscopic modelling of walking behaviour*. PhD thesis, Delft University of Technology, 2016.

[46] S.P. Hoogendoorn, S. Luding, P.H.L. Bovy, M. Schreckenberg, and D.E. Wolf. *Traffic and Granular Flow 03*. Springer, 2005.

[47] M. Campanella, S. Hoogendoorn, and W. Daamen. Quantitative and qualitative validation procedure for general use of pedestrian models. In *Pedestrian and Evacuation dynamics*, pages 892–905. Springer International Publishing, 2014.

[48] J.C. Silveira Jacques, J. Musse, and C. Jung. Crowd analysis using computer vision techniques. *IEEE Signal Processing Magazine*, 27:66–77, 2010.